NASA TECHNICAL MEMORANDUM

NASA TM-77587

ON VORTEX BURSTING

H. Werlé

Translation of "Sur l'eclatement des tourbillons", Office National D'Etudes et de Recherches Aérospatiale (ONERA), Technical Note No. 175, 1971, 50 pp.

NATIONAL AERONAUTICS AND SPACE ADMINISTRATION
WASHINGTON, D.C.
JUNE 1984

STANDARD TITLE PAGE

1. Report No. NASA TM- 77587	2. Government Accession No.	3. Recipient's Catalog No.
4. Title and Subtitle: ON VORTEX BURSTING		5. Report Date: June 1984
		6. Performing Organization Code
7. Author(s): H. Werlé, Chief of Research Group at ONERA		8. Performing Organization Report No.
		10. Work Unit No.
9. Performing Organization Name and Address: Leo Kanner Associates, Redwood City, California 94063		11. Contract or Grant No. NASw-3541
		13. Type of Report and Period Covered: Translation
12. Sponsoring Agency Name and Address: National Aeronautics and Space Administration, Washington, D.C. 20546		14. Sponsoring Agency Code

15. Supplementary Notes

Office National D'Etudes et de Recherches Aérospatiales (ONERA) Technical Note No. 175, 1971, 50 pp.
(N72-19328)

16. Abstract

The phenomena of vortex bursting has been pointed out for the first time in 1960, in "La Recherche Aéeronautique"; since then it has been the subject of many theoretical and experimental papers. Now it is studied mostly by means of visualization.

In this manner, the physical behavior of the phenomenon is emphasized, and its similarity with boundary layer separation or wake bursting becomes apparent. The essential influence of an increasing pressure gradient on the initiation, the position and the type of bursting is clearly confirmed.

Lastly, the evolution of the phenomena as a function of several parameters is analyzed in the case of delta wings, alone or installed on aircraft models; and compared with the results of similar wind tunnel or flight tests.

17. Key Words (Selected by Author(s))	18. Distribution Statement: "Unclassified-Unlimited"		
19. Security Classif. (of this report): "Unclassified"	20. Security Classif. (of this page): "Unclassified"	21. No. of Pages: 66	22.

TABLE OF CONTENTS

ON VORTEX BURSTING

H. Werlé
Chief of Research Group at ONERA

Summary

The phenomenon of vortex bursting has been pointed out for the first time in 1960, in "La Recherche Aéronautique"; since then it has been the subject of many theoretical and experimental papers. Now, it is studied mostly by means of visualization. /2*

In this manner the physical behavior of the phenomenon is emphasized, and its similarity with boundary layer separation or wake bursting becomes apparent. The essential influence of an increasing pressure gradient on the initiation, the position and the type of bursting is clearly confirmed.

Lastly, the evolution of the phenomenon as a function of several parameters is analyzed in the case of delta wings, alone or installed on aircraft models, and compared with the results of similar wind tunnel or flight tests.

I. Introduction /3

Since 1954 [4], experiments have clearly demonstrated the savage disorganization which affects the vortices of a Delta wing at high incidences: see figure 1d.

Nevertheless, it has been necessary to wait for the article [5] making its appearance in 1960 in order to see the phenomenon of bursting of vortices made the object of a series of investigations whose list has not ceased to expand since that date [5] to [50].

*Numbers in the margin indicate pagination in the foreign text.

All these results concern, on the one hand, theoretical studies, and on the other hand, experimental investigations of fundamental or applied (delta wings) nature, all carried out with the objective of explaining the phenomenon, predicting its appearance, or determining its consequences.

A critical review, even brief, of the set of these papers departs from the framework of this technical note, whose bibliography probably includes involuntary omissions for which the author begs the indulgence of the interested parties in advance.

The present contribution to the study of bursting is based primarily on observations during low velocity tests carried out in the ONERA hydrodynamic tunnel [51], whose placement into service goes back to the first tests of flows on wings in deflection [1], [2], and [3].

An initial series of tests emphasizes the analogy between the behavior, before an antagonistic pressure gradient, of a boundary layer, wake, and vortex nucleus. The processes used allow us to delicately analyze the physical arrangment of the phenomena and to distinguish different types of bursting.

A second series of experiments extends the study begun in [4] and [63]; it concerns apex vortex bursting on delta wings alone and equipping airplane models. These models are compared to those of similar tests in wind tunnels or in flight.

This steady state study is then repeated on several models in motion: rotation simulating spin, pitching oscillations, vertical bombardment motion, etc.

Finally, several tests carried out at the ONERA R1 wind tunnel of the Chalais Meudon Center allow us to formulate some remarks on the subject of vortex bursting in supersonic flow.

II. Test Means and Methods

The majority of visualizations presented in this note have been obtained in the hydrodynamic tunnel of Châtillon, whose characteristics, performances, and experimental possibilities have been published several times with numerous test examples [51].

It thus suffices to recall that this water wind tunnel is arranged vertically and without return, that it functions simply under the effect of gravity and by bursts (blowing off): see figure 1a.

With these conditions, the maximum velocity V_o obtained with its normal stream (cross-section: 220x220) never exceeds 20 cm/s. The length of this stream with its extension exceeds 1.2 m, which justifies the placement toward the back of the model and their retraction toward downstream of the attached elements of the mounting, such as the obstacles (plates normal with velocity V_o) or rectangular or circular air intakes which have the objective of modifying the pressure gradient downstream of the model: figure 1b and 1c.

With this last mounting, the flow captured by the air intake is controlled by a valve-gyrometer assembly placed on the evacuation circuit.

This arrangement has been used during the majority of basic experiments described in chapter III.

In regard to the models themselves, their attachment in the stream /4
varies according to the type of flow studied:
-in flat current, mounting between two flat walls; in certain cases, these walls have also been removed or extended in order to avoid perturbations due to the separation of boundary layers on these walls: for example figure 1b;
-in three dimensional flow, and particularly in the case of Delta wings, mounting in the rear tip or on the streamlined under surface strut: for example figures 19 and 23; in several isolated cases, half-model attached to the wall (figure 1d and 28).

The study of flow around certain models in motion has necessitated more complex mountings justifying not only the transmission of the desired motion to the model and the change of attitude (incidence, sideslipping), but also the use of the processes of visualization adopted (passage of the dye to the model, observation of the model downstream): see the examples appearing in views 30a and b (rotation), 31i (pitching oscillations), and 32a (bombardment).

The methods of visualization, for a long time described in [51] and illustrated by numerous films [63], [64], and [65], are based:
-on the one hand, on emissions of colored liquid (density one) demonstrating thin current streams even in the vicinity of the models (figure 1d and 13). We note that judicious selection of the position of the transmitter shafts on the model limits visualization to certain peculiarities of the flow (for example emission at the apex of the Delta wing revealed the axis of these vortices), which facilitates referencing of the plates obtained with their position in relaiton to the model. Moreover, placement in instantaneous course (or even the sudden stop) of these colored emissions is made the object of a recording on film [64] and large scale analysis of the images of these films allows us to follow at the time of their debut the displacement of dye and to measure the local veolcity, for example on the vortex axis, as this has been carried out during earlier studies [52] and [53];
-on the other hand, with the use of tiny air bubbles in suspension in the water precisely defin. within the entire field, the aspect of the current lines (for example, figure 2) and also that of the velocity vectors (photographed with short exposure time: for example, figure 4). For this process, illumination limited to thin slices of longitudinal or transversal flow following the cases:

-following the plane of symmetry of the mounting in planar current (for example figure 2a, c, etc.);

-following the diametral plane in rotational flow (for example, 2b, d, etc.);

-following the axis of vortices or normal to these axes in three-dimensional flow (for example, figure 9 and 16). In this last case, it is only a question of pseudo-flow in the slice considered.

These processes of visualization normally used in steady regime have been able to be applied to unsteady cases without much difficulty (for example, figure 30 to 32), with simply some restrictions inherent with this regime:
-the colored thin streams emitted by the models only represents by chance the current lines, but generally provide correct information on the absence or presence of flows, vortices, and possibly their bursting;
-the air bubbles whose trajectories only coincide with the current lines, continue to reveal the presence of vortices, flows, or wakes.

III. Fundamental Experiments Emphasizing the Analogy Between the Phenomenon Affecting the Boundary Layers, Wakes, and Vortices Issuing From a Model [65]

All these basic experiments have taken place in permanent regime and at low velocity. With a mean Reynolds number $Re \simeq 10^4$, the upstream flow was stable, uniform, completely laminar, and exempt from any wake or spurious boundary layer.

III.1. Boundary Layer Separation Before an Obstacle Creating an Antagonistic Gradient /5

We note first of all that the character of laminarity of the flow around models is clearly demonstrated by air bubbles with trajectories correctly staged, any turbulence resulting in disordered trajectories.

In planar current, the laminarity of the boundary layer along the model is also revealed by the presence of a layer without bubbles (and appearing in black on the plates). It is thus along a flat wall without obstacles (figures 2a).

In rotational flow, this black layer can not be observed on the axial cylinder by reason of its small diameter (figure 2b).

In both cases, a projection of the wall induces separation of the boundary layer and a separated zone with mixed character, that is to say laminar upstream and turbulent downstream, to develop before the

solid obstacle constituted by the projection (figure 2c and d).

The boundary layer of a wall also separates when the antagonistic pressure gradient is due to a fluid obstacle, such as it forms before an air intake functionning with low flow coefficient: $V_E/V_o \simeq 0.5$ (figure 2e and f).

We find with these conditions the standard arrangement of generalized separation, similar to that which we observe on a curved wall forming a divergence with high slope (figure 2g and h).

The curves of figure 3 deduced from measurements carried out on the test plates and films precisely define the evolution of the separation point before the projection as a function of the velocity V_o (Re) and the dimensions of the model in planar current (figure 3a) and rotational flow (figure 3b).

They confirm nevertheless that the separation point recedes when the flow captured by the air intake increases (figure 3c and d).

III.2. Sound Flow Before an Obstacle Creating an Antagonistic Gradient

The behavior of a sound flow exempt from any wake or vortex in the presence of an antagonistic gradient is illustrated by figure 4. The experiment confirms that no separation can be detected in before the obstacle constituted by the plate normal to the wind (figure 4a and b) or the air intake functionning at low flow (figure 4c and d), whether this is in planar current or rotational flow.

The trajectory elements described by the bubbles during the relatively short exposure time of the images taken during tests have allowed us to deduce the law of velocity along the mounting axis before the plates (figure 5a and b) and the air intakes (figure 5c and d), and to note in this last case their evolution as a function of the flow coefficient.

These curves characterize the antagonistic gradient existing before the solid or fluid obstacles thus arranged in the stream.

III.3. Wake Bursting Before an Obstacle Creating an Antagonistic Gradient

In planar current, the confluence of two laminar boundary limits at the flight edge of a thin plate without incidence (figure 6) gives birth to a wake which extends the model (wake which appeared in black on the plates obtained with the air bubble method).

In the absence of any obstacle effect (figure 6a and b), this wake, first rectilinear and stable, becomes downstream the center of undulations or even staggered vortices which ensure stirring with formation of a turbulent wake.

An obstacle placed on the trajectory of the wake before its complete homogenization induces its bursting (figure 6b and f) at a point which we can characterize as being the start of the divergence of the wake: see plan (figure 6d). It then forms before the obstacle a separated fluid pocket within the flow. This pocket has a turbulent character and its boundary is the center of vortices carried by the current. /6

When the distance of the obstacle downstream of the flight edge of the upstream plate decreases (figure 6c) or when the flow captured by the air intake decreases (figure 6g), the bursting point recedes upstream and the separated pocket which it gives rise to develops.

At the boundary, the bursting point rejoins the flight edge of the model and the boundary limits on this plate end by separating before arriving at the flight edge (figure 6g).

On the curves of figure 7, we note displacement of the bursting point (x_1) as well as that of the apex of the separated fluid pocket (x_2) as a function of the flow coefficient of the intake (figure 7a and b) and the BdF-obstacle distance (figure 7c), as well as the influence of velocity V_o (Re).

We do not fail to note the similarity existing between the evolution of the bursting point of a wake (figure 7) and that recorded for the separation point of a boundary layer (figure 2).

III.4. Vortex Bursting Before an Obstacle Creating an Antagonistic Gradient

After a certain number of unsuccessful attempts with more or less elaborate vortex chambers and sometimes having points in common with those described in [16], [20], [26], [41] and [50]; the mounting represented on figure 1c is finally the only one which has allowed us to obtain isolated steady vortex within a fluid stream to nearly uniform within a test stream without notable spurious effects due to the walls or mounting elements.

The vortex in question is that which forms at the free end of a straight thin half-plate of low aspect ratio (λ=2) and mounted to the wall.

This marginal vortex, of which we can vary the intensity by modifying the wing incidence, is particularly stable and well ordered at average incidences and does not burst in the absence of any obstacle effect (figure 8a).

On the other hand, a solid obstacle placed on its trajectory disorders it and induces its bursting (figure 8b and c). As in the case of the wake described in III.3, the same phenomenon is also observed in front of an air intake functionning at low flow (figure 8d).

These visualizations with colored emissions can be confirmed by the views of the same phenomenon obtained with the assistance of air bubbles (figure 9a, b and c), and particularly in longitudinal (following the vortex axis) and transversal (perpendicular to the axis upstream and downstream of the bursting point) section planes.

All these experiments emanate from the plan of the phenomenon

(figure 9d, e and f):
-the vortex nucleus, steady and quasi-rectilinear near the wing, deforms in order to come to surround a separated fluid pocket within the flow;
-it then takes the form of a helix of increasing diameter, but coiled in inverse direction of the vortex;
-this helix turns around its axis which extends this from the non-bursting nucleus and in the same direction as the vortex.

The bursting point can be defined as the point of the axis where the divergence of the nucleus begins, that is to say where this last loses its steady character.

As in the case of a wake (III.3), vortex bursting is a phenomenon whose appearance, extension, and position in relation to the airfoil can in large measure be controlled by adjustment of the antagonistic gradient (position of the obstacle plate normal to the wind, functionning regime of the air intake): see figure 10.

The experimental curves of figure 11 obtained with these conditions precisely defines the displacement of the bursting point toward upstream under the effect of an increasing obstruction ($V_E/V_o \searrow$) for different values of the velocity V_o (Re) of the flow (figure 11a) and incidence i of the model (figure 11b).

These results are in agreement with those given on figure 7. However, an examination carried out from test film images taken with the assistance of the intermittent colored emissions described in chapter II has provided the law of velocity V_a along the axis of the vortex nucleus upstream of the bursting point (figure 12a). /7

We observe that this velocity remains at first approximately equal to 0.6 V_o, then falls abruptly enough to zero at the moment of arrival at the bursting point.

We record on the other hand translation toward upstream of this curve when the velocity V_o (Re) or the obstruction effect of the air

intake (figure 12b) increases.

The visualizations and curves obtained with the hydrodynamic tunnel do not allow us to proceed with verification of the theory elaborated by H. Squire [9] (vortex bursting when its maximum circumferential velocity in the transversal plane is equal to 1.22 times the axial velocity) or that established by H. Ludwieg [29] (vortex bursting when the slope of current lines at the edge of the nucleus reaches 42^{o}).

III.5. Types of Bursting Observed on a Delta Wing

At high incidences, the apex vortices on the upper surface of a Delta wing burst naturally [6] and [63].

In the case of an airfoil without side-slipping and a moderate leading edge camber (figure 13a), we know that the two principal vortices are separated by a median zone of non-vortical sound flow [52] and [64] which avoids any interaction. With these conditions, their bursting also is produced at equal distance from the apex.

When the leading edge camber is higher or the incidence greater, the median sound zone between the two vortices disappeared and the equilibrium between the bursted zone became unstable (figure 18e, g and h) [21].

The presence of a small obstacle in the bursted wake of vortices suffices to make its bursting point recede upstream and to delay the bursting of the second vortex (figure 13c).

The inverse phenomenon is recorded when the obstacle is replaced by a shaft which allows us to delay considerably or even avoid completely bursting (figure 13b) [52] and [63].

When we arrange behind a non-side-slipping Delta wing an air intake with rectangular cross-section in view of simultaneously acting on the two vortices of the upper surface, we can, as this has been done

above, modify the pressure gradient in a case where it induces naturally the bursting (figure 14b and c).

As previously, bursting recedes toward the apex by developing when the air intake creates an obstruction effect (figure 14a).

On the other hand, progressive increase of the flow captured by the intake makes the phenomenon evolve in the following manner:
-retreat toward downstream of the bursting which continues to give birth to a separated fluid pocket, indefinite and with mixed character, analogous to the generalized separation which is produced on a wall (figure 14d);
-resorption of the separated pocket which closes by conserving its mixed character, comparable to the localized separation called "bulb" which we sometimes observe at the leading edge of a shape (figure 14e) [51] and [70];
-disappearance of the turbulent character of the finite separated pocket which becomes the equivalent of a laminar bulb (figure 14f);
-finally, complete resorption of the bursting phenomenon (figure 14g).

This evolution only confirms the observations of N. Lambourne [30]. The closing of the bursted vortex at the downstream end of a finite fluid pocket represents the inverse phenomenon of bursting or "implosion" of the vortex.

Its analogy with the well known phenomenon of sticking together of a flow on a planar or cylindrical wall under the effect of a favorable gradient is obvious (see figure 15a, c, e and g), as it is also with the closing of a wake into a confluence point within the fluid, whose visualized examples are rarer (figure 15b, d, f and h) [53].

IV. Physical Study of Natural Bursting of Vortices of Delta Wings

IV.1. Mechanism of Bursting

In spite of the reduced scale of the phenomenon, the experimental

work confirms for the principal vortices of a thin Delta wing with sharp edges, accentuated camber, and high incidence (figure 16), the mechanism of bursting such that it has been able to be magnified and released by the preceding fundamental experiments.

Moreover, the intermittent colored emissions method has allowed us to record the evolution of the velocity along the axis of the vortices (figure 17) since besides this had already been carried out earlier for non-bursted vortices of Delta wings [52] and [64].

The curves obtained reveal that the velocity along the axis increases rapidly in the vicinity of the apex, passes through a maximum by clearly exceeding in coefficient the velocity V_o, finally decreases by falling abruptly to zero at the bursting point. This decrease is on the contrary very progressive when the vortex does not burst.

IV.2. Influence of the Reynolds Number

The experiment confirms once again that the Reynolds number does not have any notable influence on the mechanism of upper surface side vortical flow when it is a question of wings in accentuated camber and with sharp edges. This is true for the range: $0.5 \cdot 10^4 \leq Re_1 \leq 5.3 \cdot 10^4$ tested by varying either the dimensions of the model (length of chord 1) or the velocity V_o of the current (figure 18).

The influence of this parameter on the curves of velocity on the axis is given by figure 17a: the maximum attained by this velocity is even higher when the Reynolds number is higher, thus confirming the earlier results [52].

However, when the Reynolds number increases, the bursting point tends recede slightly toward upstream, but this displacement remains since we observe it on figure 22a in the interval of dispersion of numerous results acquired in wind tunnels with clearly higher Reynolds numbers [10], [24], [47] and [49].

IV.3. Influence of Incidence

When the incidence of a Delta wing increases, bursting of its vortices generally makes its appearance at a certain distance from the edge of the airfoil flight, then progressively goes back to pass along the upper surface and come up to the proximity of the apex.

This evolution is illustrated by the plates of figure 19.

Concerning the law of variation of the velocity along the vortex axis, the higher the incidence, the more it presents a high and prominent maximum, and the more this maximum itself approaches the apex (figure 17a): on the Delta wing tested ($\varphi_{BA}=75^{o}$), it is located at $x=0.65\ l_a$ for $i=25^{o}$ and culminates at $x=0.26\ l_a$ for $i=40^{o}$.

On the other hand, figure 20 precisely defines the position of the bursting point at different incidences and compares the curves obtained with the hydrodynamic tunnel without and with correciton of the obstruction effect due to the model at the considerable incidences attained, with results of measurements in wind tunnels [11] and [49], etc. on Delta wings of the same camber ($\varphi_{BA}=75^{o}$) and Reynolds numbers 100 times greater. We note the good coincidence of the corrected curve of the tunnel with the points obtained by D. Hummel [26].

Nevertheless, a similar comparison can be carried out on figure 22a in the case of a lower camber ($\varphi_{BA}\cong 65^{o}$). If the curve recorded with the tunnel places itself sufficiently well within the midst of the relatively dispersed results acquired in wind tunnels [10], [24], [47] and [49], it extends contrarily to the preceding ones up to moderate incidences ($10^{o} < i < 20^{o}$) and with a less marked variation of slope. /9

IV.4. Influence of Bursting

As figure 1 demonstrates in the case of a Delta wing with a camber $\varphi_{BA}=65^{o}$ and placed at 20^{o} incidence, the influence of pitching on the

position of the bursting point of vortices is significant.

When j increases from 0^{o}, the equilibrium is destroyed: bursting develops and approaches the apex on the half-wing which sees its leading edge camber decrease ($\varphi_{Eff}=\varphi_{BA}-j$), and on the contrary the phenomenon recedes toward downstream or even ceases to be produced from the opposite side.

The curves of figure 22b give the displacement as a function of j of the bursting point for three values of the incidence. This evolution is confirmed by tests carried out in wind tunnel on an airfoil whose leading edge camber is on the same order [47].

IV.5. Influence of Leading Edge Camber

If we compare at constant incidence and zero pitching a series of Delta wings with decreasing edge cambers, we observe the phenomenon of bursting of their vortices progress from downstream to upstream.

In order to maintain the phenomenon in a given relative position, it is necessary to reduce the incidence of the airfoil progressively and with measurements which decrease the leading edge camber (figure 23).

With these conditions, the curves of figure 24 relative to displacement of the bursting point as a function of the incidence for Delta wings having different leading edge cambers (j=0) all have the same aspect and correctly rise by stages.

From all these results, we have taken the two curves of figure 25 which give the variation as a function of the camber φ_{BA}, the critical incidence i_E for which the bursting of vortices is situated at the edge camber (or at mid-chord) of the airfoils. Even there the experimental points obtained in wind tunnels [11], [25], [39] and [49] generally cluster around the curves acquired with the hydrodynamic tunnel.

IV.6. Influence of Thickness of the Outline and the Planar Shape (BdF)

A comparison between the upper surface vortices of a series of Delta wings ($\varphi_{BA}=60^{o}-j=0^{o}$) whose radius of the leading edge and thickness of the outline varies, can be carried out on figure 26.

The incidence of the models has been selected in a fashion to place the bursting point of the vortices either in the vicinity upstream of the flight edge (figure 26a, c, e and g) or at the height of the mid-chord (figure 26b, d, f, and h).

In both cases, the values obtained increase considerably when the bevel of the leading edge, first limited to the upper surface, becomes symmetrical, then when the thickness of the outline increases and the stopping of the leading edge disappeared.

The influence of the planar shape from the rear portion of the airfoil has been studied in the case of a thin Delta wing with sharp edges placed at 20^{o} incidence and without pitching (figure 27).

It appears that neither the old-fashioned shape, delta or with double-camber of the rear tip, nor the contra-camber of the flight edge had any notable action on the position of the vortices and their bursting. On the other hand, the presence of a narrow strip placed at the flight edge without deflection under the vortex (figure 27d) suffices to obtain retreat of the bursting point as it acted with a larger wing (figure 27e).

IV.7. Influence of a Jet Emitted Following the Vortex Axis /10

The idea of using a jet directed along the vortex axis of a Delta wing is not new [6], but its systematic study had not been undertaken until having proven the effectiveness of a lateral jet as a means of reducing or suppressing separations, particularly on a straight wing of high incidence [55] and [67].

Figure 28 demonstrates the application of the process in the case of a Delta wing ($\varphi_{BA}=60^{o}-i=25^{o}$): we note that the turbulent jet emitted at the mid-chord downstream of the bursting point has the effect not only of delaying the appearance of bursting and reordering the vortex, but also of bending this last toward the rear point by considerably extending the median round and non-vortical portion of the bursting at the expense of the eddy zone which usually develops at the rear point.

IV.8. Bursting on Airplane Models with Delta Airfoils

All the preceding results acquired with airfoils alone have been able to be extended to the case of more complex airplane models with camber wings, on which the jet engines were simulated (figure 29) [40] and [54]. The existence of the phenomena observed with the hydrodynamic wind tunnel have been confirmed with several repetitions through flight tests, particularly in the case of the Douglas F5D airplane [31] and [66] and with that of the Concorde airplane [61] and [71].

IV.9. Bursting on Models in Motion

Bursting around a model carried along in uniform rotation in order to represent a roll or spin motion is illustrated by figure 30 [68].

The motion is transmitted to the model mounted on its rear tip through the intermediary of a ring which allows observation following the axis of the stream with a mirror placed downstream at 45^{o} (figure 30a and b).

Uniform rotational motion around the axis of a thin Delta wing without incidence or pitching (figure 30c) makes two symmetrical vortices appear in relation to this axis, that is to say on the upper surface of the descending half-wing and on the lower surface of the ascending half-wing [56]: all this occurs as if the effective incidence of the descending half-wing was increased and that of the ascending half-wing decreased.

In the case of a model inclined on the stream V_o, the vortical effects due to the rotation superimpose on those which result from the incidence; with these conditions, we observe the development of the vortex along the descending leading edge, and on the contrary, partial or even complete resorption of the vortex along the ascending leading edge (figure 30d and e).

These results extend to the case of high incidences where we observe that the bursting of vortices well depends on the local incidence (retreat of the phenomenon from the side of the ascending half-wing). On the other hand, they remain valid in the case of complete airplane models (figure 30j and k).

A second example is that of a model propelled by periodic motion of pitching oscillations. Figure 31i reveals the mounting on the rear tip and a portion of the mechanism used for modulation of the incidence i following an approximately sinusoidal law (indeed, the system adopted produced besides a motion of rolling oscillations).

A comparison between the steady regime (fixed incidence) on figure 31a, b, c and d, as well as on figure 31 j, and the non-steady regime (variable incidence) on figure 31e, f, g and h, on the one hand, and 31k to r on the other hand, demonstrates that the non-steady vortices are more developed and more turbulent, that at any moment they occupy a position clearly closer to the leading edge, that this is on a Delta wing alone or on an airplane model including a fuselage.

These observations confirm the results of similar tests carried out in wind tunnels by N. Lambourne [57].

Figure 31 reveals besides that in non-steady, bursting is maintained on the second half of the Delta wing ($\varphi_{BA}=60^o$), although it does not recede beyond the flight edge in the case of the airplane model (higher camber). With these tests, the amplitude of the oscillations ($\pm 5^o$) is far from being as low as that ($\pm 1^o$) of similar tests carried out in windtunnels by L. Woodgate [60]. /11

A last case of non-steady bursting is illustrated by figure 32. It concerns a model propelled by a periodic motion of translation normal to the stream, called bombardment motion, which a rack-bar device transmits to it (figure 32a).

The mechanism has been tested with a single airfoil (figure 32b, c, and d) and with an airplane model of Concorde type (figure 32e, f, g, h, i and j) [61] and [71].

During the descending phase of the cycle, the effective incidence of the model finds itself increasing, although it decreases at the time of climbing; this is why we alternately observe accentuation of the vortex regime of the upper surface, then its partial or even complete resorption; simultaneously, we observe climbing of the bursting point toward upstream, then its retreat or even its disappearance.

During the descending phase (figure 32d, g and j), the altitude of the vortices above the airfoil is clearly higher than in permanent regime at the equivalent effective incidence, this is that which was revealed from similar tests carried out in wind tunnels, particularly by R. Maltby [58] and G. Moss [59].

IV.10. Remarks on the Subject of Supersonic Bursting

In supersonics [62] and [69], bursting on the upper surface of a Delta wing with incidence conserves the vortical structure which it possesses in incompressibility. In order to demonstrate it, we generally call on methods of strioscopic or parietal (induced) visualization. Pressure probings carried out in the transversal planes normal to the wing often complete these images and allow us to better interpret them, and to locate well certain details, as for example the axis of the vortices at the boundary of a dark sector issuing from the apex.

When at high incidences, the bursting of vortices is produced, this phenomenon is more difficult to distinguish on strioscopic views.

The study of bursting of vortices based on such observations has been tackled for the first time at Mach 2 by A. Craven and A. Alexander [19]. Previously B. Elle [5] had done it at high subsonics (M=0.9). The tests at Mach 1.95 undertaken with the ONERA R1 wind tunnel subsequently have had the objective of precisely defining the phenomenon and their evolution under the effect of perturbation (figure 33).

Even at moderate incidence, it appears that the vortices of apex disorder before the shock wave issuing from the flight edge (figure 33a). A shock plane issuing from a dihedral placed above the Delta wing and adjustable in position and inclination induces perturbation which allows us to obtain artificial displacement of the bursting point toward the apex (figure 33d), even at lower incidence (figure 33c).

The same result can be obtained without the dihedral artifice by means of a notable increase of the incidence (figure 33b): bursting of the vortices then climbs toward the apex without the shock wave of the flight edge being the cause.

Figure 34 allows us to compare the distributions of pressure of stopping obtained in a transversal plane situated upstream of the flight edge during tests without dihedral:
-on the one hand, at 25° incidence, thus upstream of the bursting point;
-on the other hand, at 30° incidence, being downstream of this point.
The considerable extension of the surface of the vortex nucleus does not allow any doubt to remain on the existence of the phenomenon.

V. Conclusion

From the study which came to be made, we defined the following principal results:
-bursting of the vortices constitutes an example of boundary layer separation or wake bursting, one of the fundamental phenomena of fluid mechanics; /12
-it is a question of sudden disorganization which can be generalized or localized, and have a laminar or turbulent or even mixed type character;

-bursting manifests itself as well in incompressibility as in compressibility, in subsonics as well as in supersonics, in steady as well as non-steady regime; its appearance and position depend at the time on local conditions and the general antagonistic pressure gradient;
-natural bursting observed on the camber wings and on airplanes with Delta airfoils at high incidences is basic ; governed by the interaction effects which can be produced between the two principal vortices, or under the effect of shafts (air intakes) and jets (jet engine exits), or even under the action of obstacles (drift) or of lateral blast (pitching); these effects do not pose serious problems for balancing and high-lift of aircraft.

REFERENCES

/13

1. Roy, M., "Characters of flow around an accentuated camber wing", C.R.Ac.Sc. 234, 2501-2503 (1952)

2. Legendre, R., "Flow in the vicinity of the point upstream of a high camber wing with average incidences", Rech. Aéron. 30 (1952) and 31 (1953).

3. Werlé, H., "Visualization in hydrodynamic tunnel", Rech. Aéron. 33 (1953).

4. Werlé, H., "Some experimental results on camber wings, at low velocities, obtained in hydrodynamic tunnel", Rech. Aéron. 41 (1954).

5. Elle, B.J., "An investigation at low speed of teh flow near the apex of thin delta wings with sharp leading ledges", ARC R & M 3176 (January 1958).

6. Werlé, H., "On the bursting of vortices of apex of a delta wing at low velocities", Rech. Aéron. 74 (1960).

7. Elle, B.J., "On the breakdown at high incidences of the leading edge vortices on delta wings", J.A.R.S. (August 1960).

8. Jones, J.P., "The breakdown of vortices in separated flow", USAA Rep. 140, July 1960.

9. Squire, H.B., "Analysis of the "vortex breakdown" phenomenon", Part 1 Imperial college Rep. 102, 1960.

10. Lambourne, N.C. and D.W. Bryer, "The bursting of leading-edge vortices: some observations and discussion of the phenomenon", ARC R & M 3282 (April 1961).

11. Earnshaw, P.B. and J.A. Lawford, "Low speed wind-tunnel experiments on a series of sharp-edged delta wings", (Part 1) RAE T.N. 2780 (1961) and ARC R & M 3424 (1964).

12. Lawford, J.A. and A. Beauchamp, "Low speed wind-tunnel measurements on a thin sharp-edged delta wing 70° leading-edge sweep, with particular reference to the position of leading-edge vortex breakdown", R.A.E. T.N. Aero 2797 (1961).

13. Spence, A. and D. Lean, "Some low speed problems of high speed aircraft", AGARD Bruxelles (1961).

14. Ludwieg, H., "Zur Erklärung der Instabilität der überangestellten Deltaflügeln abtretenden freien Wirbelkerne", Z.fl Flugwiss 10 Heft 6 (1962).

15. Brooke, B.T., "Theory of the vortex breakdown phenomenon", J. of fluid mech. 14 (4) (December 1962).

16. Harvey, J.K., "Some observations of the vortex breakdown phenomenon", J. of fluid mech. 14 (4) (December 1962).

17. Jones, W.P., "Research on unsteady flow", J.A.S. 29 (3) (March 1962).

18. Gartshore, I.S., "Recent work in swirling incompressible flow", Nat. Res. Coun. of Canada-Ottawa N.R.C. No. 6968, June 1962.

19. Craven, A.H. and A.J. Alexander, "An investigation of vortex breakdown at Mach 2", The College of Aeronautics Cranfield CoA Note Aero 158, November 1963.

20. Kirkpatrick, D.L.I., "Experimental investigation of the breakdown of a vortex in a tube", R.A.E. T.N. Aero 2963 (May 1964).

21. Lowson, M.V., "Some experiments with vortex breakdown", J.R.A.S. (May 1964).

22. Hummel, D., "Untersuchungen über das Aufplatzen der Wirbel an schlanken Deltaflügeln", D.F.L.-Bericht No. 0196 (1963); D.L.R. FB64-12 (1964); Z. Flugwiss 13 (1965), Heft 5.

23. South, P., "A simple theory of vortex bursting", Nat. Res. Coun. of Canada Aero. Rep. LR-414, 1964.

24. Earnshaw, P.B., "Measurement of vortex-breakdown position at low speed on a series of sharp-edged symmetrical models", RAE T.N. 64047 (November 1964).

25. Poisson, Q.P. and E. Erlich, "Lift increase and balancing of slender wings", AFITAE Colloquium, November 1964; NASA TT-F-9523 (August 1965).

26. Chanaud, R.C., "Observations of oscillatory motion in certain swirling flows", J. Fluid Mech. 21 (1) (1965). /14

27. Hummel, D., "Experimentelle Untersuchung der Strömung auf Saugseite eines schlanken Deltaflügels, Z. Flugwiss 13 (1965), Heft 7.

28. Richards, E.J., "Aeronautical Research at the University of Southampton", J.R.A.S. 656 (August 1965).

29. Ludwieg, H., "Erklärung des Wirbelaufplatzens mit Hilfe der Stabilitätstheorie für Strömungen mit schraubenlinienförmigen Stromlinien", Z. Flugwiss 13 (December 1965), Heft 12.

30. Lambourne, N.C., "The breakdown of certain of vortex", ARC CP 915 (September 1965).

31. Rolls, S, D. Koenig and F. Drinkwater, "Flight investigation of the aerodynamic properties of an ogee wing", NASA T.N.D. 3071 (December 1965).

32. Brooke, B.T., "Some developments in the theory of vortex breakdown", ARC 27945 AD 642179 (April 1966).

33. Hall, M.G., "On the occurrence and identification of vortex breakdown", R.A.E. T.R. 66 283 (August 1966).

34. Logan, A.H., "A solution to the vortex breakdown phenomena in a trailing line vortex", University Park, Pennsylvania, December 1966.

35. Hall, M.G., "A new approach to vortex breakdown", Proceedings of the 1967 heat transfer and fluid mechanics institute, Stanford University Press, 1967.

36. Wentz, W. and M. McMahon, "Further experimental investigations of delta and double delta wing flow fields at low speeds", NASA Contr. Rep. CR 714, February 1967.

37. Parkinson, G.V., Y.C. SUN and H.R. Davis, "Observations on low aspect ratio wings at high incidence", Canadian Aeronautics and Space Journal (March 1967).

38. Din-Yu, H., "On the shock transition, the hydraulic jump and vortex breakdown", California Inst. of Tech. Pasadena Div. of Eng. and Appl. Science Rep. 85-39, March 1967.

39. Hummel, D. and P.S. Srinivasan, "Vortex breakdown effects on the low speed aerodynamic characteristics of slender delta wings in symmetrical flow", J.R.A.S. 71 (April 1967).

40. Poisson, Q.P. and H. Werlé, "Water tunnel visualization of vortex flow", Astronautics and Aeronautics (May 1967).

41. So, K.L., "Vortex phenomena in a conical diffuser", AIAA Journ. 5 (6) (June 1967).

42. Bossel, H., "Inviscid and viscous models of the vortex breakdown phenomenon", University of California Report No. AS-67-14 (1967).

43. Das, A., "Zum anschwellen aufgerollter Wirbelflächen und Aufplatzen des Wirbelkerns bei schlanken Tragflügeln", Z. Flugwiss 10 (October 1967).

44. Hummel, D., "Zur Umströmung scharfkantiger schlanker Deltaflügel bei grossen anstellwinkeln", Z. Flugw. 10 (October 1967).

45. Earnshaw, P.B., "Measurements of the effects of thickness on vortex breakdown position on a series of sharp-edged delta wings", RAE T.R. 68050 (February 1968).

46. Wentz, W., "Wind tunnel investigation of vortex breakdown on slender sharp-edged wings", NASA CR-98737 (November 1968).

47. Hummel, D. and G. Redeker, "On the influence of vortex breakdown on the aerodynamic coefficients of low-aspect ratio delta wings in yaw", Boeing Co. Translation No. B 859 (1969) after WGLR Jahrbuch 1967.

48. Leibovich, S., "Wave motion and vortex breakdown", AIAA Paper No. 69-645 Fluid and Plasma Dynamics Conference, San Francisco, California, June 1969.

49. Wentz, W.H. and D.L. Kohlman, "Vortex breakdown on slender sharp-edged wings", AIAA Paper No. 69-778 Aircraft design and operations meeting, San Francisco, California, June 1969.

50. Cassidy, J. and T. Falvey, "Observations of unsteady flow arising after vortex breakdown", J. Fluid Mech. 41 (4) (1970).

51. Werlé, H., "Insight on the experimental possibilities of the hydrodynamic visualization tunnel of ONERA", Technical Note No. 48, 1958.

52. Werlé, H., "Physical study of the vortical phenomena with the hydrodynamic tunnel", ATMA Communication (1961 session) and Werlé, H., "Vortices of very slender thin wings", Rech. Aérosp. 109 (1965).

53. Werlé, H., "Separation and joining of fluid flows", Rech. Aeron. 70 (1960).

54. Werlé, H. and C. Fiant, "Hydrodynamic visualization of the low speed flow around an airplane model of the "Concorde" type", Rech. Aérosp. 102 (1964).

55. Cornish, J.J., "High lift applications of spanwise blowing", ICAS, Seventh Congress, Rome, September 1970.

56. Harvey, J.K., "A study of the flow field associated with a steadily rolling slender delta wing", J.R.A.S. (February 1964).

57. Lambourne, N.C., "Some current and proposed investigations into the flow for slender delta and other wings in unsteady motion", ARC 21 844 (April 1960).

58. Maltby, R.L., P.B. Engler and R.F. Keating, "Some exploratory measurements of leading-edge vortex positions on a delta wing oscillating in heave", R.A.E. T.N. Aero 2903 (July 1963).

59. Moss, G.F., "Further analysis of measurements of leading edge vortex position on a delta wing oscillating in heave", R.A.E. T.N. Aero 2903A (September 1964).

60. Woodgate, L., "Measurements of the oscillatory pitching-moment derivatives on a sharp-edge delta wing at angles of incidence for which vortex breakdown occurs", N.P.L. Aero 1275 (July 1968).

61. Werlé, H., "Visualizaiton of the ground effect at low velocity around an airplane model", Rech. Aérosp. 1970-2 T.P. ONERA 834 (1970).

62. Monnerie, B. and H. Werlé, "Study of the supersonic and hypersonic flow around a thin wing with incidence", AGARD C.P. No. 30, London (May 1968); T.P. ONERA No. 557 (1968).

FILM LIBRARY

63. ONERA Film 304, "Bursting of vortices at apex"(1960) (16 mm, sound, duration: 6 mn.).

64. ONERA Film 378, "Physical study of vortical phenomena" (1961) (16 mm, sound, duration: 18 mn.).

65. ONERA Film 575, "Flows with large fluctuations of velocity", (1968) (16 mm, sound, duration: 17 mn.).

66. NASA Film (Ames Research Center), "Flight test of the Douglas F5D airplane", (16 mm, silent, duration: 2 mn.).

67. ONERA Film 649, "Lateral blowing on airfoil", (1970) (16 mm, silent, duration: 5 mn.).

68. ONERA Film 485, "Flow around a delta airplane in spin", (1964) (16 mm, sound, duration: 6 mn. 30 s).

69. ONERA Film 583, "Evolution of the flow around a delta wing as a function of the Mach number", (1968) (16 mm, silent, duration: 8 mn.).

70. ONERA Film 608, "Bulb of flow at the leading edge of a airfoil outline", (1969) (16 mm, sound, duration: 4 mn.).

71. ONERA Film 412, "Simulation of the ground effect", (1970) (16 mm, sound, duration: 19 mn.).

/16

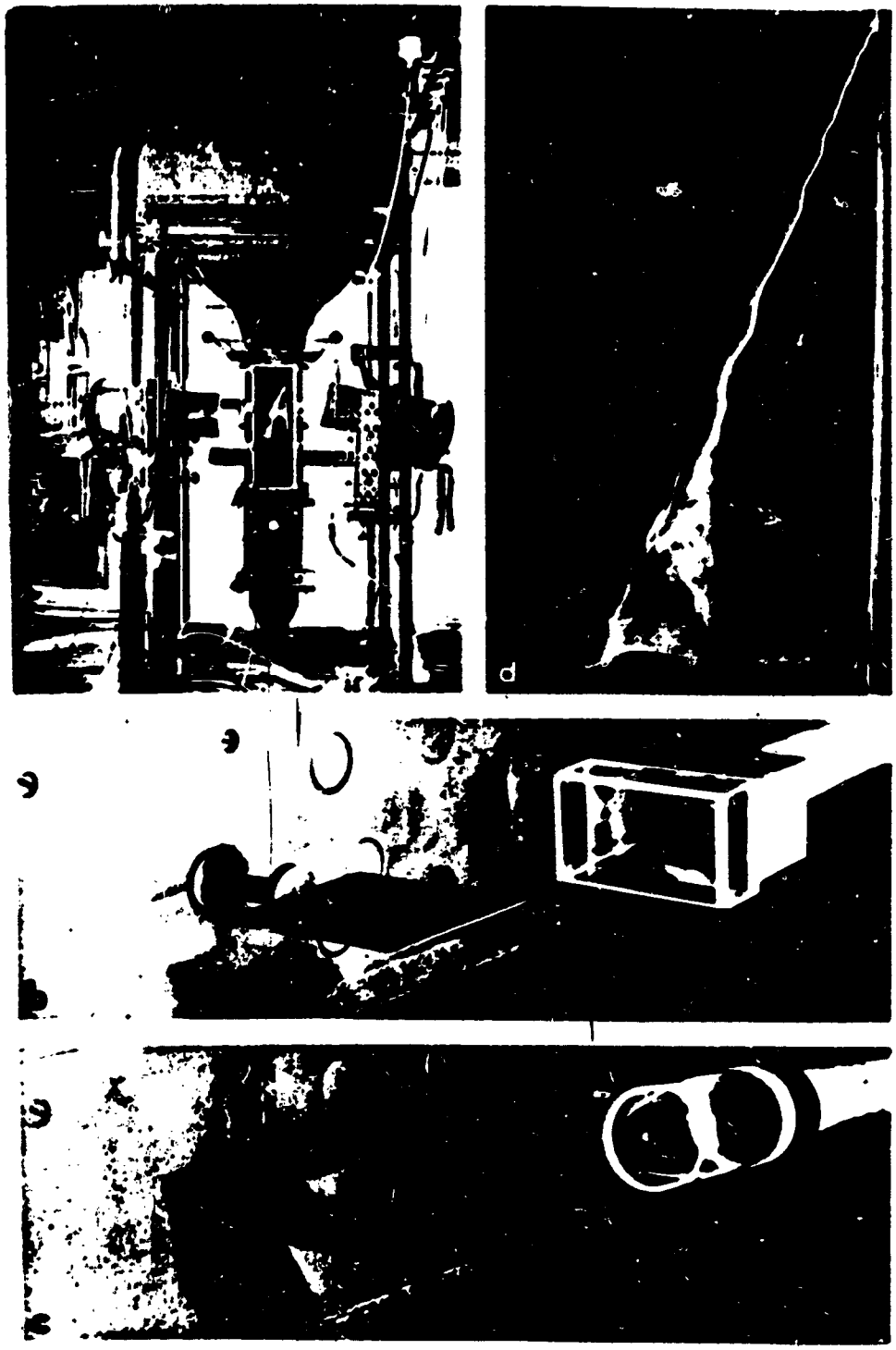

Figure 1. Test methods and mountings.

a) recent view of the hydrodynamic visualization tunnel
b) and c) examples of mountings with air intake downstream serving to control the pressure gradient and thus allowing us to operate on the wake (b) or the marginal vortex (c) of the model
d) non-induced vortex bursting of apex of a thin Delta half-wing ($\varphi_{BA}=60^{o}$; $i=17^{o}$; $Re_{la} \simeq 2 \cdot 10^{4}$) during a test carried out in 1954 and published in [4] (figure 9): visualization by colored emission.

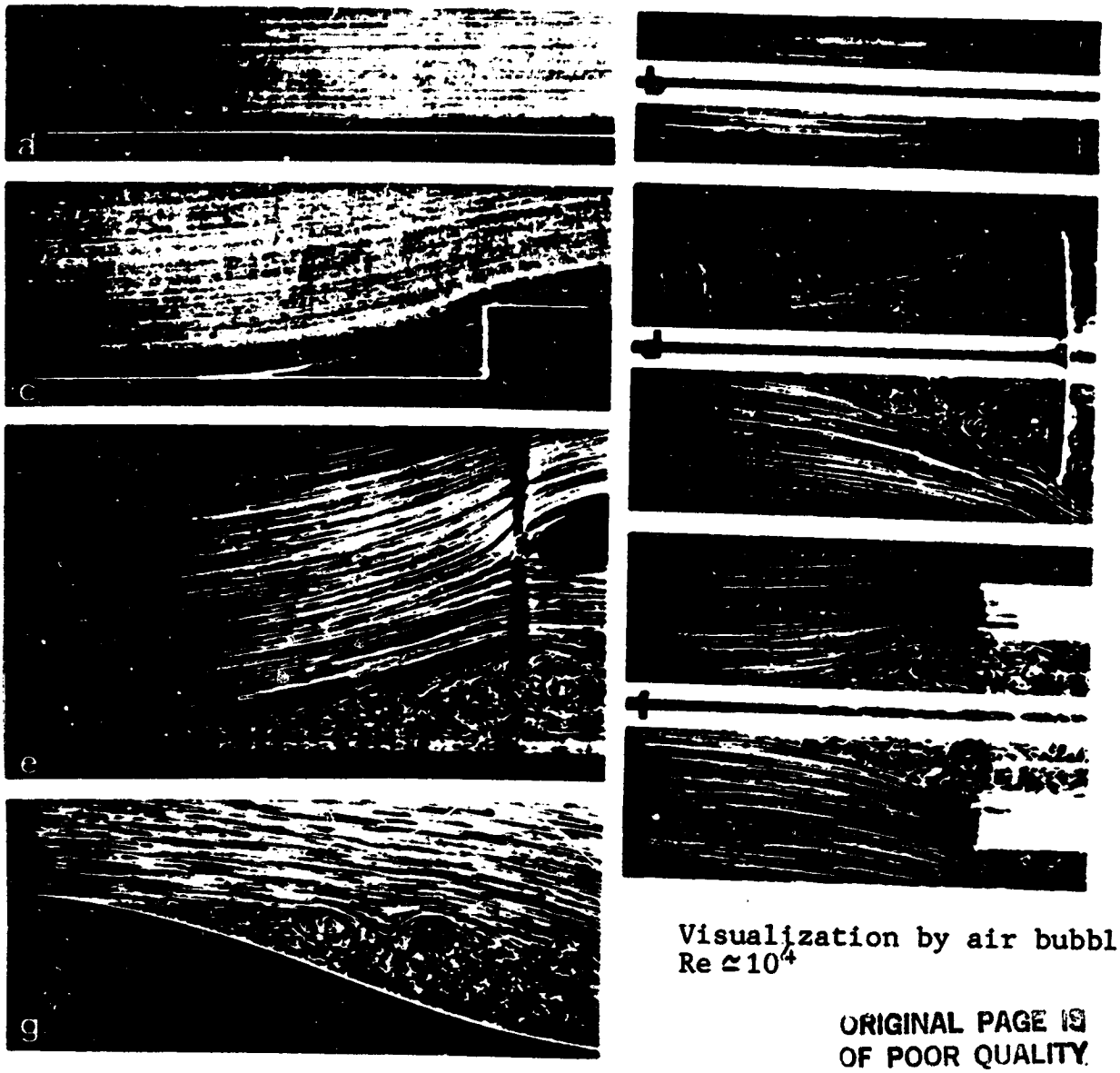

Visualization by air bubbles
$Re \simeq 10^4$

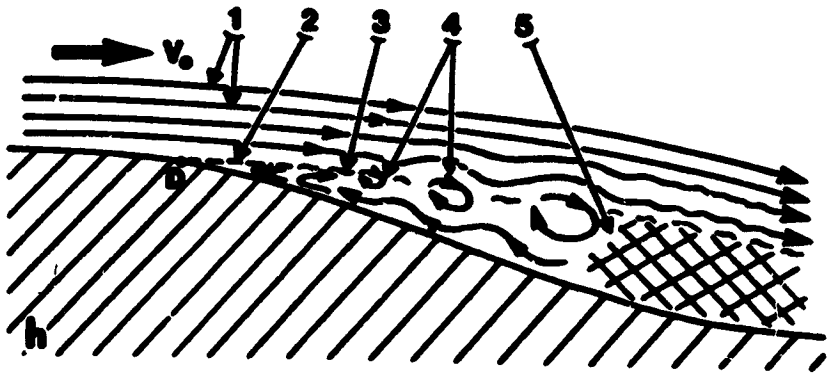

Figure 2. Separation of boundary layer along a wall in planar current (a, c, e, g and h) and in rotational flow (b, d and f).

a) and b) non separated boundary layer; c) and d) separation before an obstacle; e) and f) separation before an antagonistic pressure gradient by an air intake downstream functionning at entry $V_E \simeq 0.5\ V_o$; g) generalized separation on a curved wall forming a divergent with high slope;

Figure 2 (cont.)

h) diagram of the separated flow with generalized separation:
1=current lines (laminar flow)
2=boundary of the separated zone, stable side upstream, fluctuating side downstream
3=transition
4=vortices carried by the current
5=turbulent separated zone D-separation point (tangential or under slight angle)

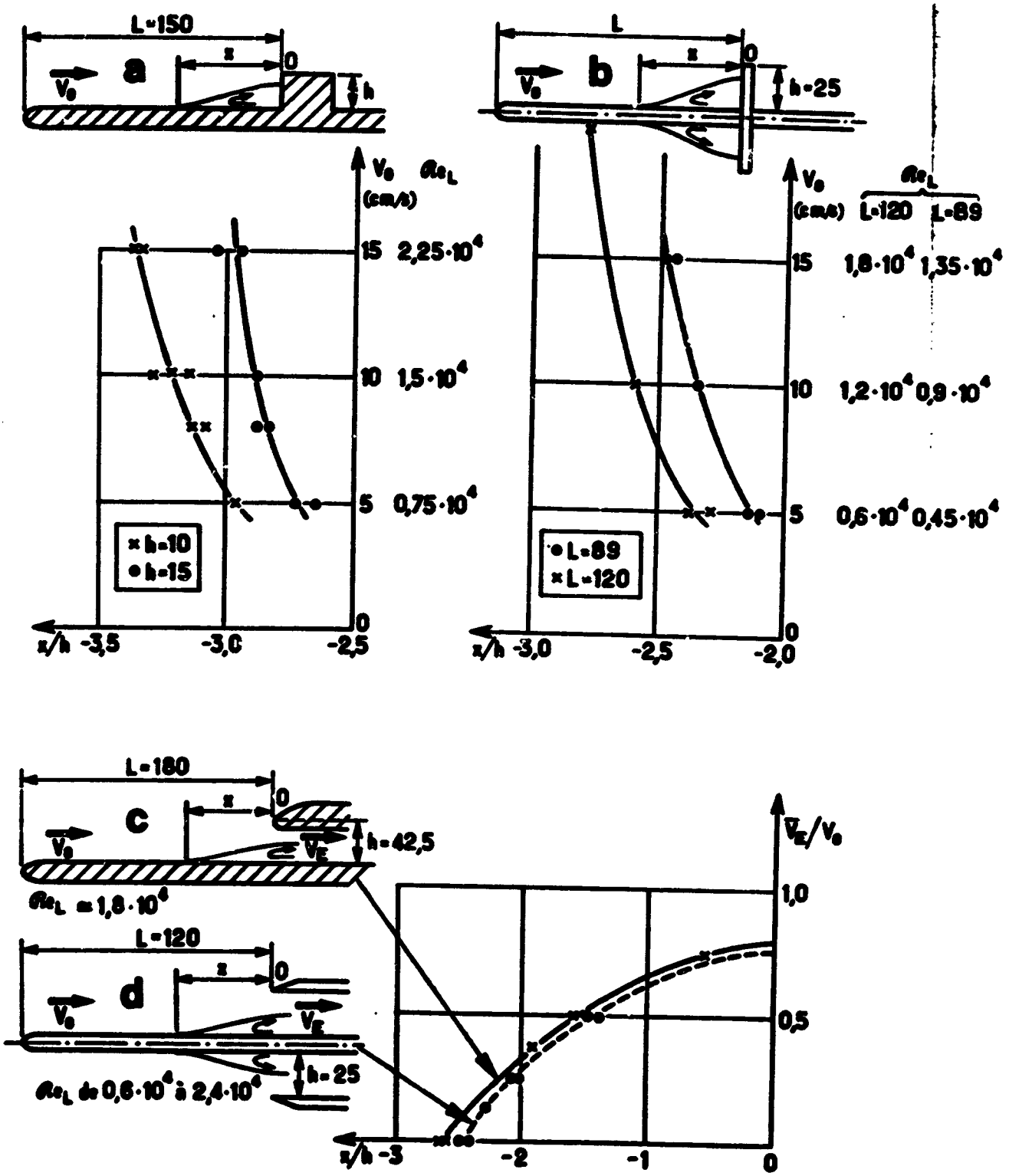

Figure 3. Evolution of separation of the boundary layer on a flat wall in planar current (a and c) and rotational flow (b and d).

a) and b) influence of velocity V_0 (Re) on separation in front of an obstacle c) and d) influence of the ratio of velocities V_E/V_0 on separation before an air intake (V_E: mean entry velocity).

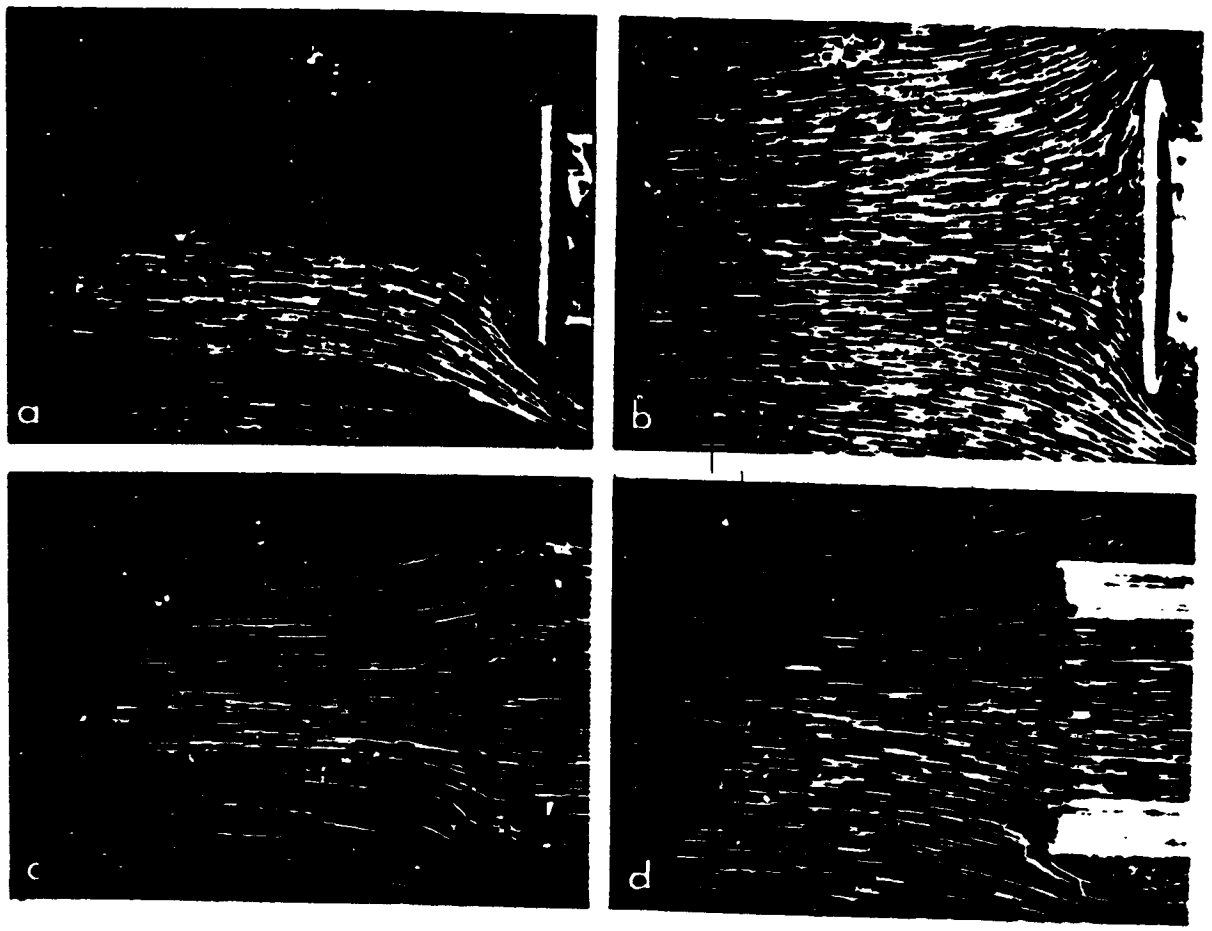

Figure 4. Flow with a vacuum stream upstream of an obstacle (a and b) and an air intake (c and d).

a) rectangular obstacle (plane of symmetry)
b) circular obstacle (diametral plane)
c) rectangular air intake (plane of symmetry
d) rotating air intake (diametral plane

$V_E/V_o \simeq 0.5$

$Re \simeq 10^4$

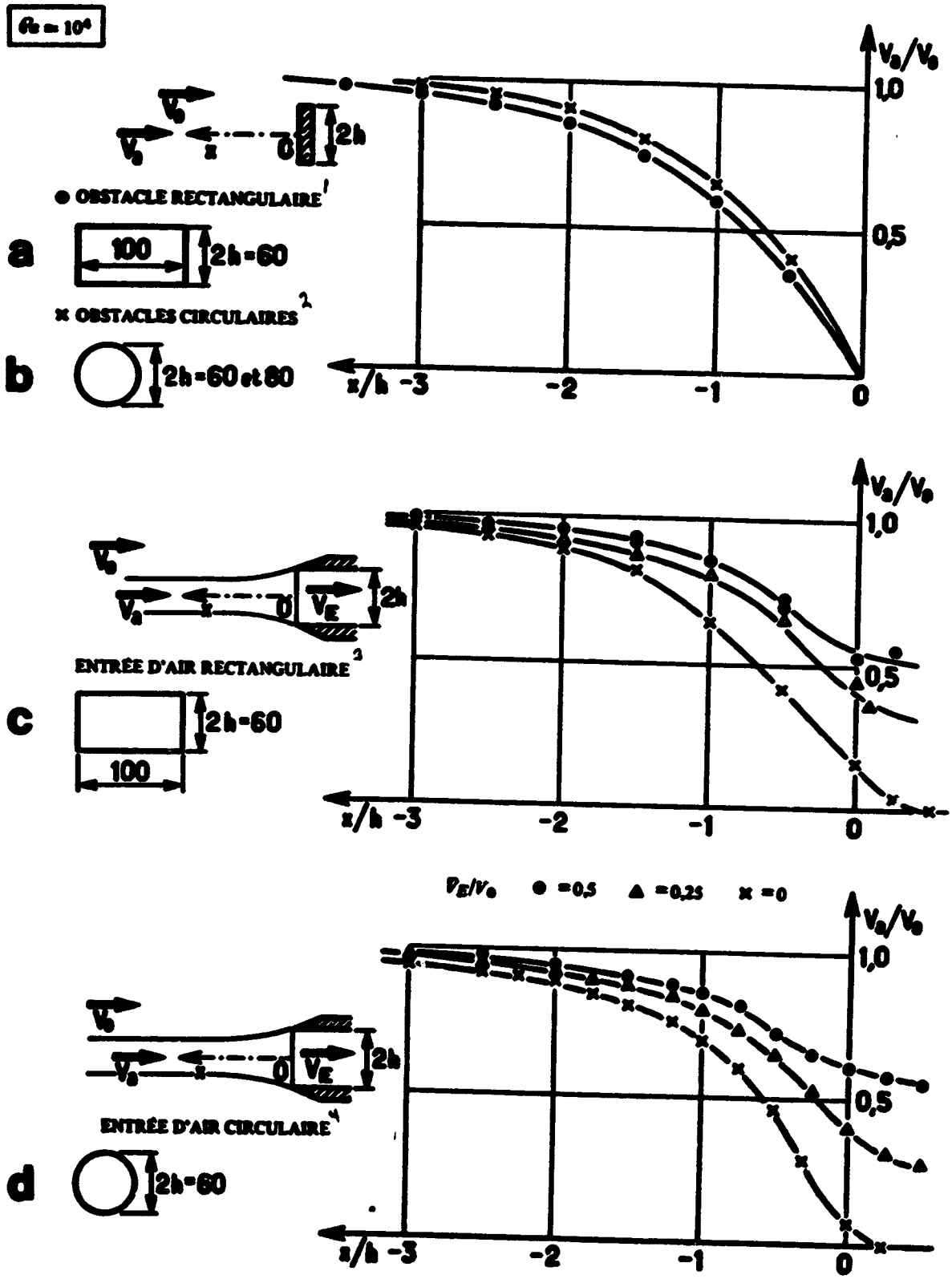

Figure 5. Evolution of the velocity along the axis of a vacuum stream upstream of an obstacle (a and b) and an air intake (c and d).

Key: 1-rectangular obstacle 2-circular obstacle 3-rectangular air intake 4-circular air intake.

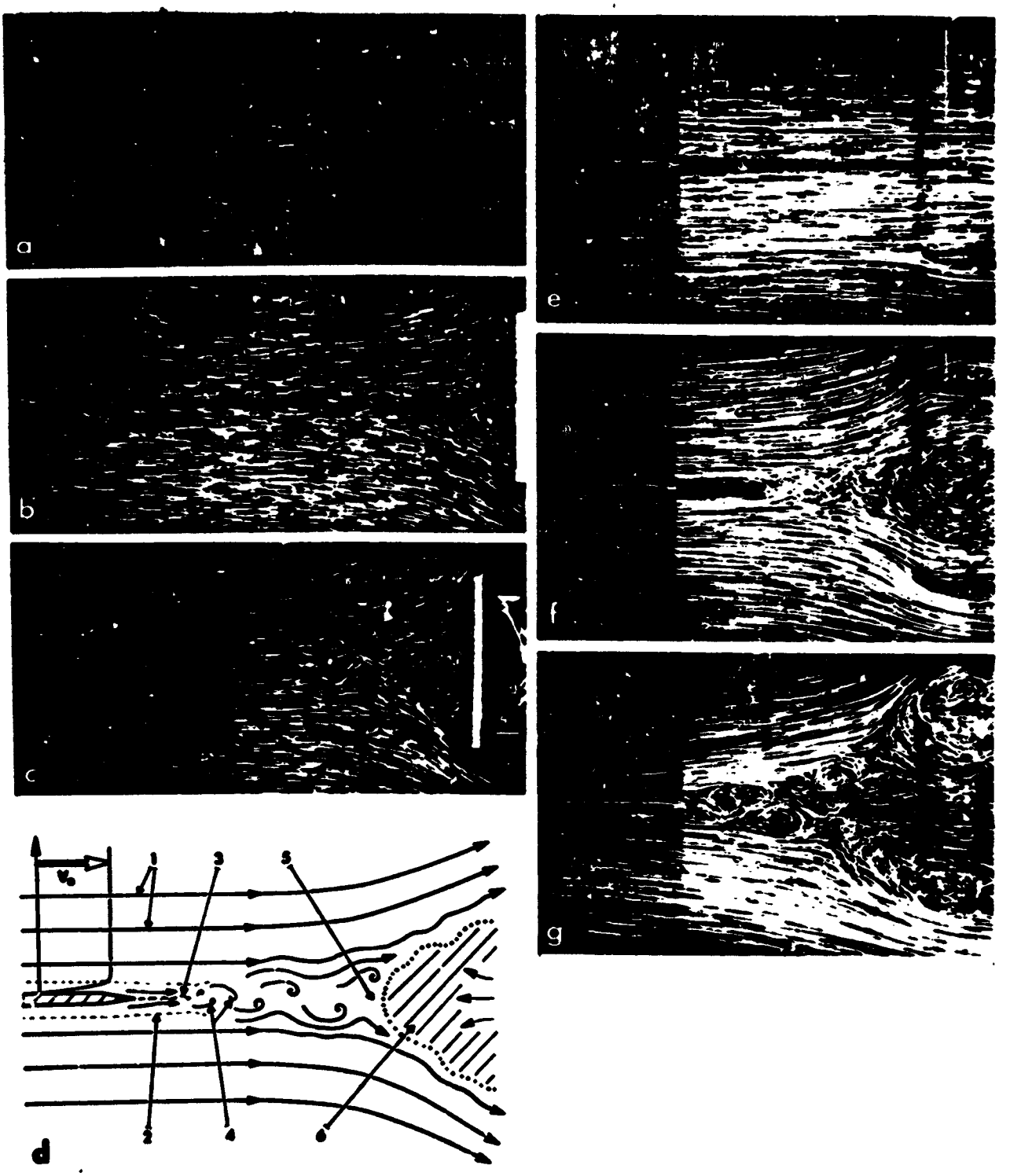

Figure 6. Wake bursting of boundary layers in planar current in front of an obstacle (a, b, c, and d) and an air intake (e, f and g).

a) non-burst wake (L=5 l) b) burst wake (L=1.7 l) c)burst wake (L=0.8 l) d) diagram of wake bursting of boundary layers: 1=current lines 2=wake boundary 3=start of wake divergence, departure point of vortices 4 4=staggered vortices carried by the current 5=pseudo-stopping at the apex of the pocket 6 6=separated fluid pocket within the fluid and with turbulent character e) non-burst wake ($V_E \simeq V_o$) f) burst wake ($V_E \simeq 0.25$ V_o) g) separation on the plate ($V_E=0$) for e), f) and g): $L \simeq 0.8$ l L=BdF-obstacle or air intake distance; chord of upstream plate l=100 $Re_l \simeq 0.75 \cdot 10^4$; i=0.

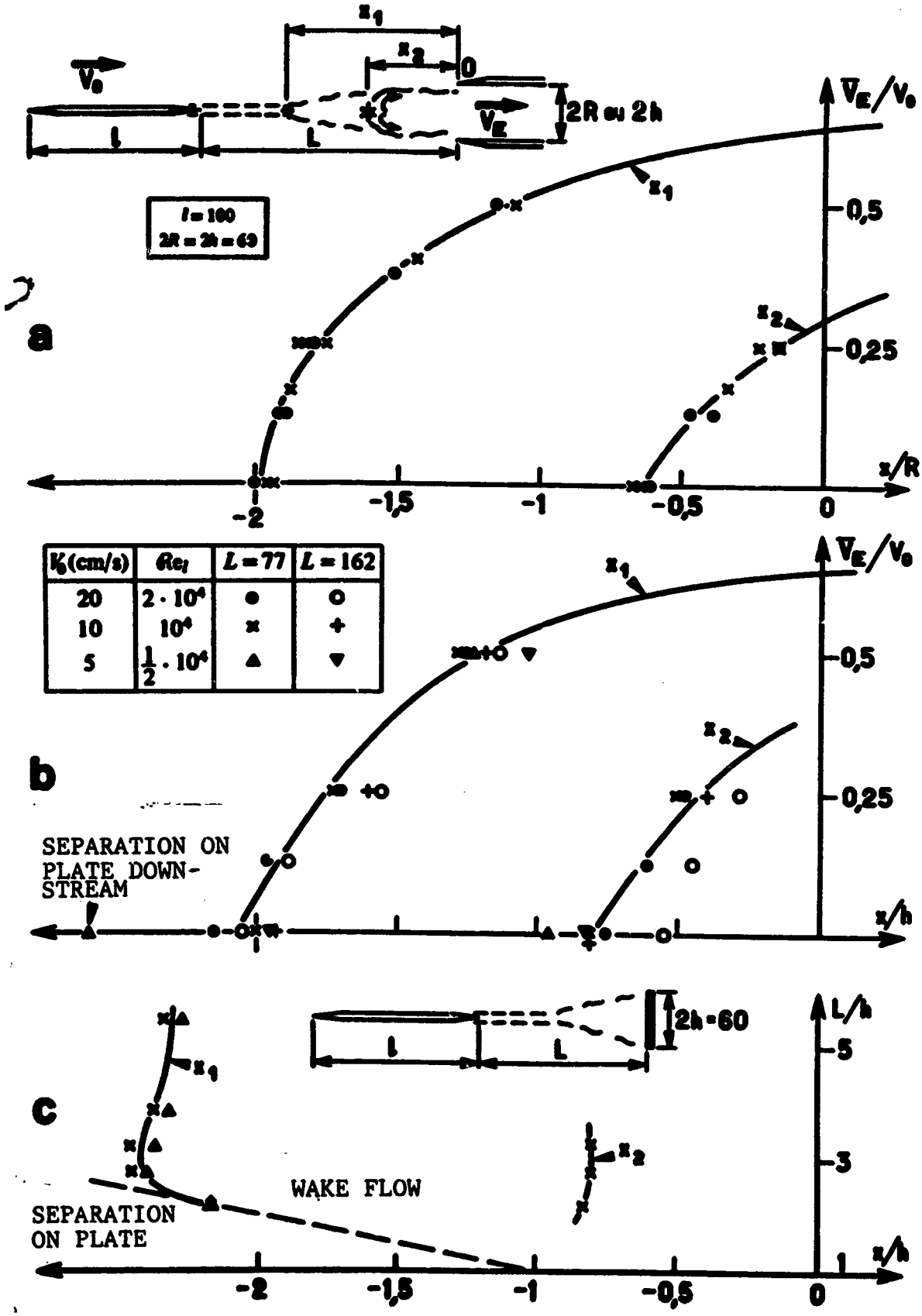

Figure 7. Wake bursting of boundary layers in front of an air intake (a and b) and an obstacle (c).

a) rotating air intake (diametral plan) } influence of the ratio
b) rectangular air intake (plane of symmetry) } of velocities V_E/V_0
c) rectangular obstacle (plane of symmetry): influence of distance L from the BdF to the obstacle.

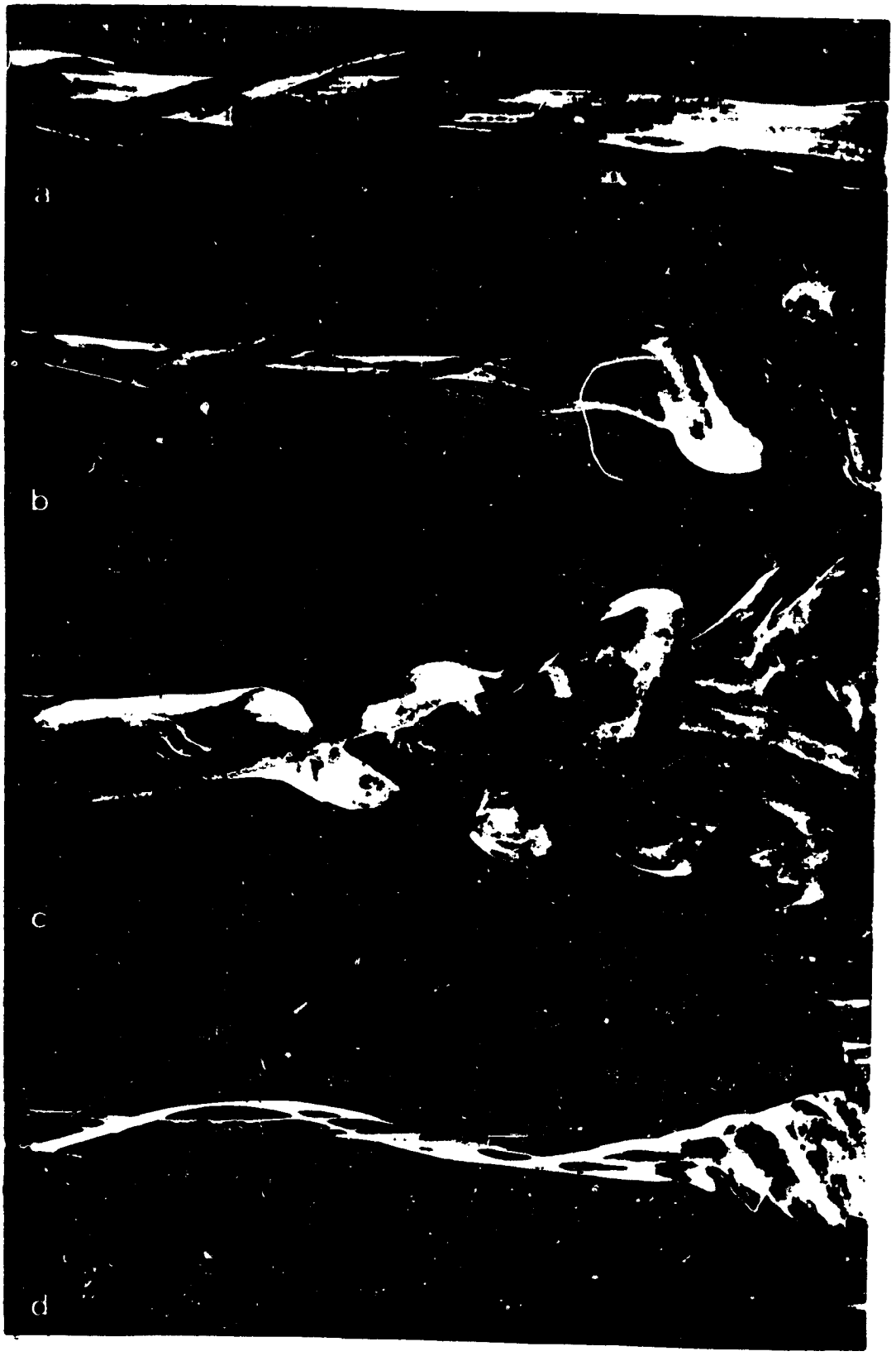

Figure 8. Vortex bursting of airfoil before an obstacle (a, b, and c) or an air intake (d).

a) non-burst vortex (L=5 l)
b) bursting before an obstacle (L=2 l)
c) bursting before an obstacle (L=1.3 l)
d) bursting before an air intake functionning at $V_E \simeq 0.5\ V_o$

} visualizaiton by colored emissions

L=BdF-obstacle or air intake distance; incidence i=12°; chord l=100 $Re_1 \simeq 0.5 \cdot 10^4$.

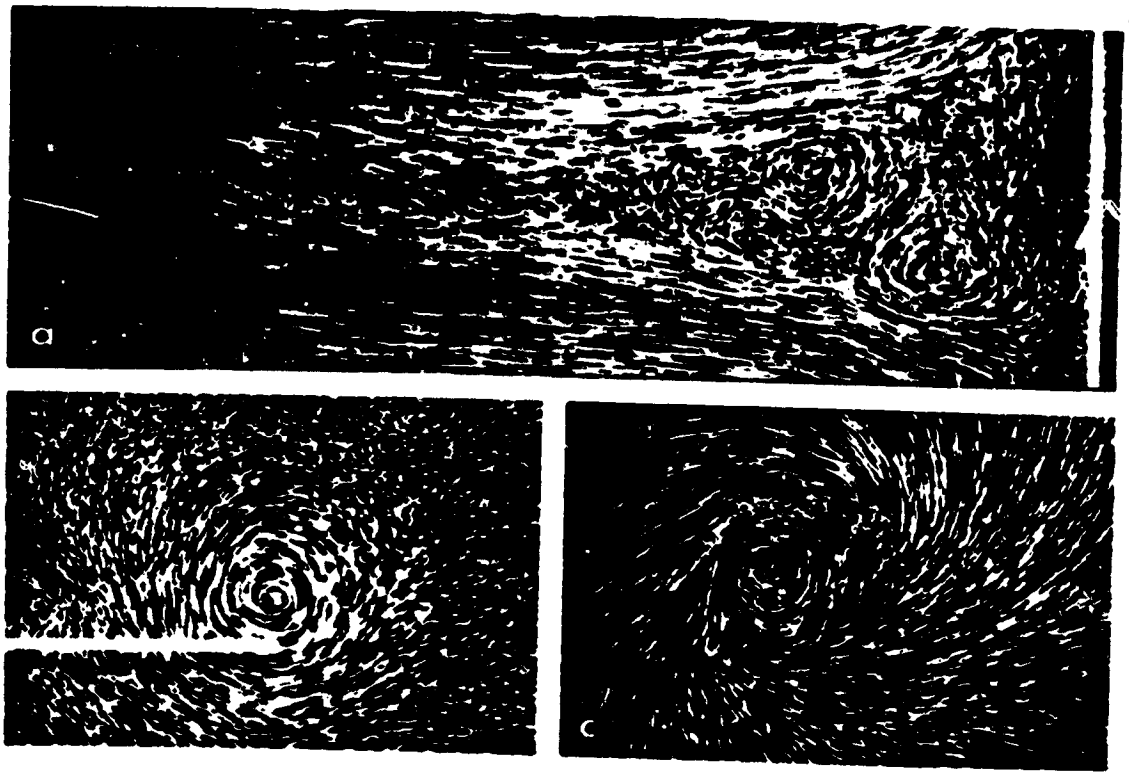

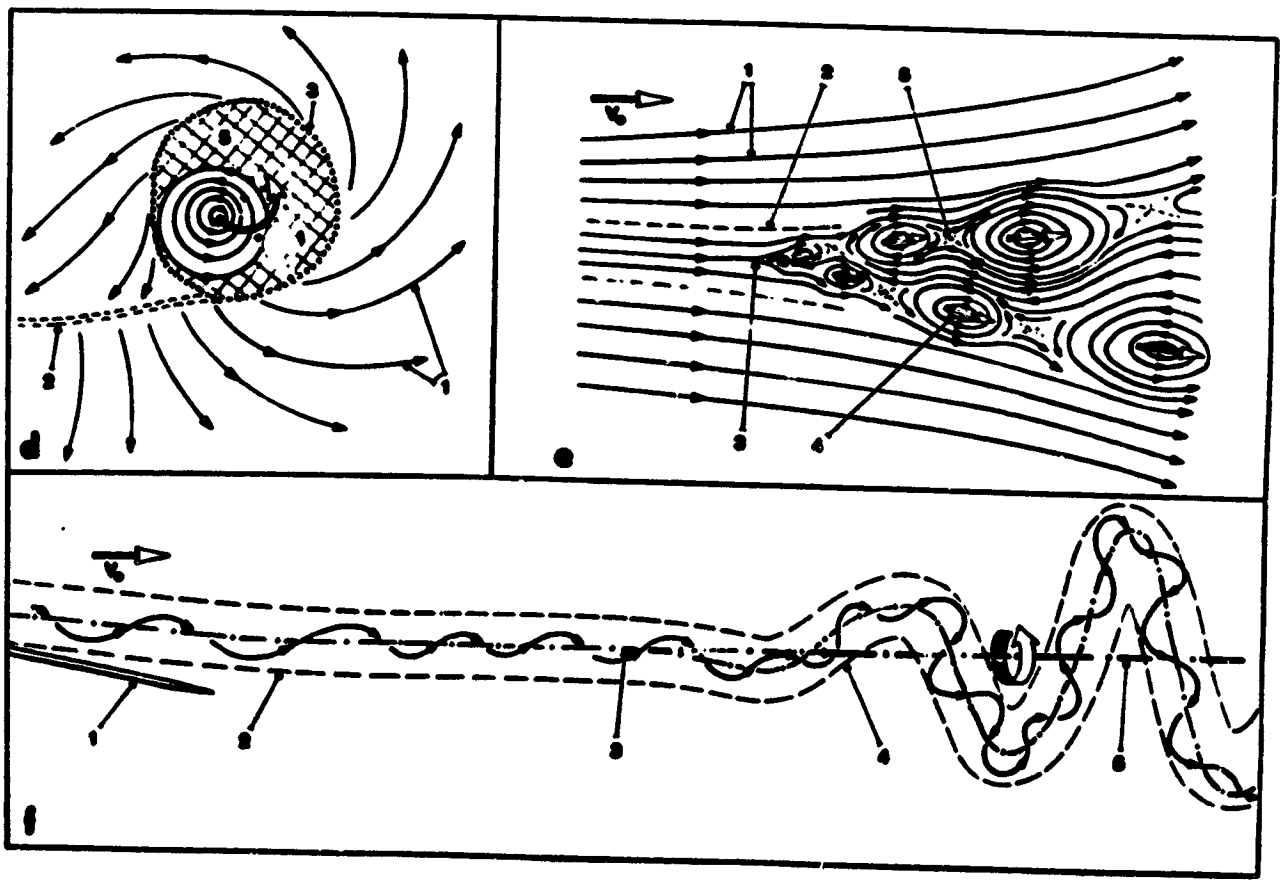

see facing page

Figure 9. Vortex bursting of airfoil before an obstacle.

a) phenomenon observed in a longitudinal plane passing through the vortex axis
b) non-burst vortex observed in the transversal plane situated at the flight edge of the airfoil
c) burst vortex observed in a transversal plane situated downstream of the bursting point

$i=12^{o}$; $L=1,3$ 1
$Re_1 \simeq 0.5 \cdot 10^4$
visualization by air bubbles

d) diagram of pseudo-flow in the transversal plane c, situated downstream of the bursting point:
1=current lines of sound flow
2=graph of the airfoil wake
3=boundary of the turbulent zone swept by the burst vortex
4=graph in the preceding zone of the vortex nucleus
e) diagram of pseudo-flow in the longitudinal plane a, passing through the vortex axis:
1=current lines of sound flow
2=boundary of the stationnary upstream and non-deformed nucleus portion
3=bursting point from which we observe deformation and rotation of the nucleus
4=graphs of the deformed nucleus in the longitudinal plane considered and having the aspect of passage of staggered vortices carried by the current
5=turbulent zone between two successive preceding graphs
f) diagram of the nucleus of a burst vortex:
1=airfoil
2=non-deformed stationnary portion of the nucleus
3=bursting point
4=nucleus portion in the form of a helix of increasing diameter and coiled in inverse direction to the vortex
5=axis around which turns the deformed part of the nucleus and which extends the axis of the non-deformed and stationnary part

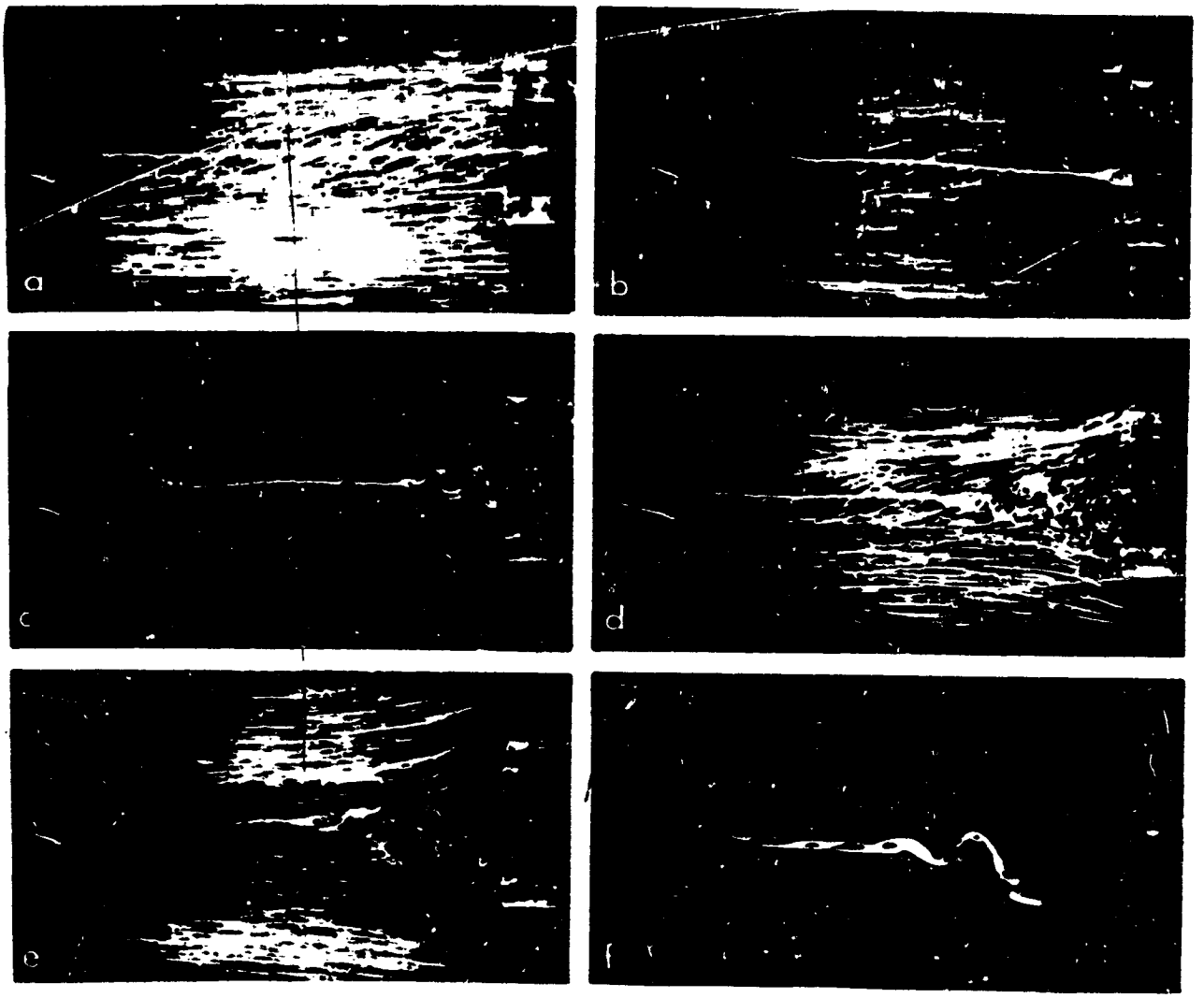

Figure 10. Evolution of vortex bursting of the airfoil ($i=12^{o}$) in front of an air intake as a function of the ratio of the velocities V_E/V_o (a, b, c, d, and e) and comparison with its bursting in front of an obstacle.

a) $V_E \simeq V_o$
b) $V_E \simeq 0.75\ V_o$
c) $V_E \simeq 0.625\ V_o$
d) $V_E \simeq 0.25\ V_o$
e) $V_E = 0$

} visualization by air bubbles of bursting in a plane passing through the vortex axis $Re_1 \simeq 2 \cdot 10^4$; L=1.651; l=100; 2R=0.61

f) $V_E = 0$ vortex axis visualized by colored emission $Re_1 \simeq 0.5 \cdot 10^4$; L=2 l; 2R=1.2 l; l=100

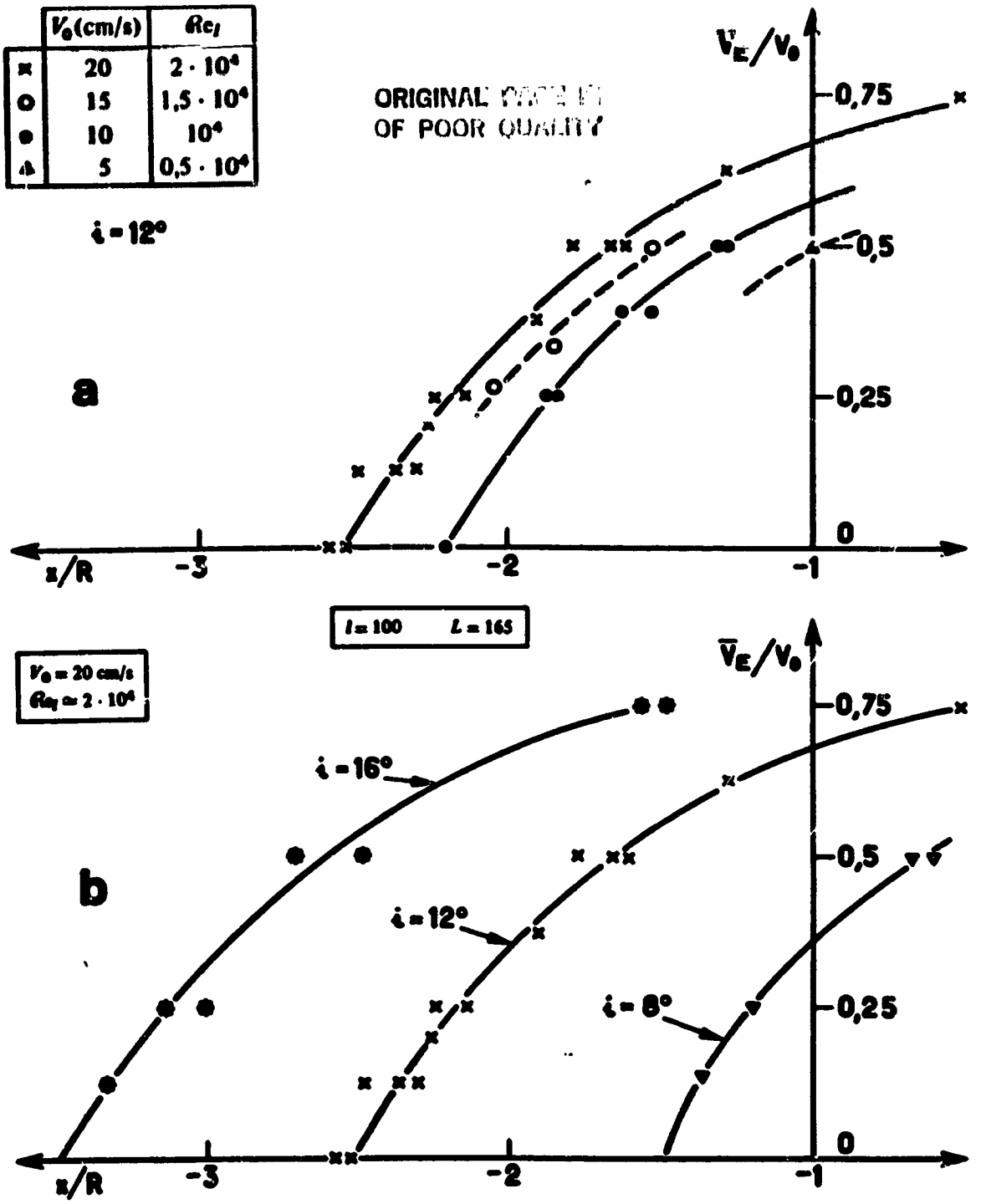

Figure 11. Evolution of vortex bursting of the airfoil before an air intake as a function of the ratio of the velocities V_E/V_o.

a) influence of velocity V_o (Re_l)
b) influence of incidence i of the airfoil

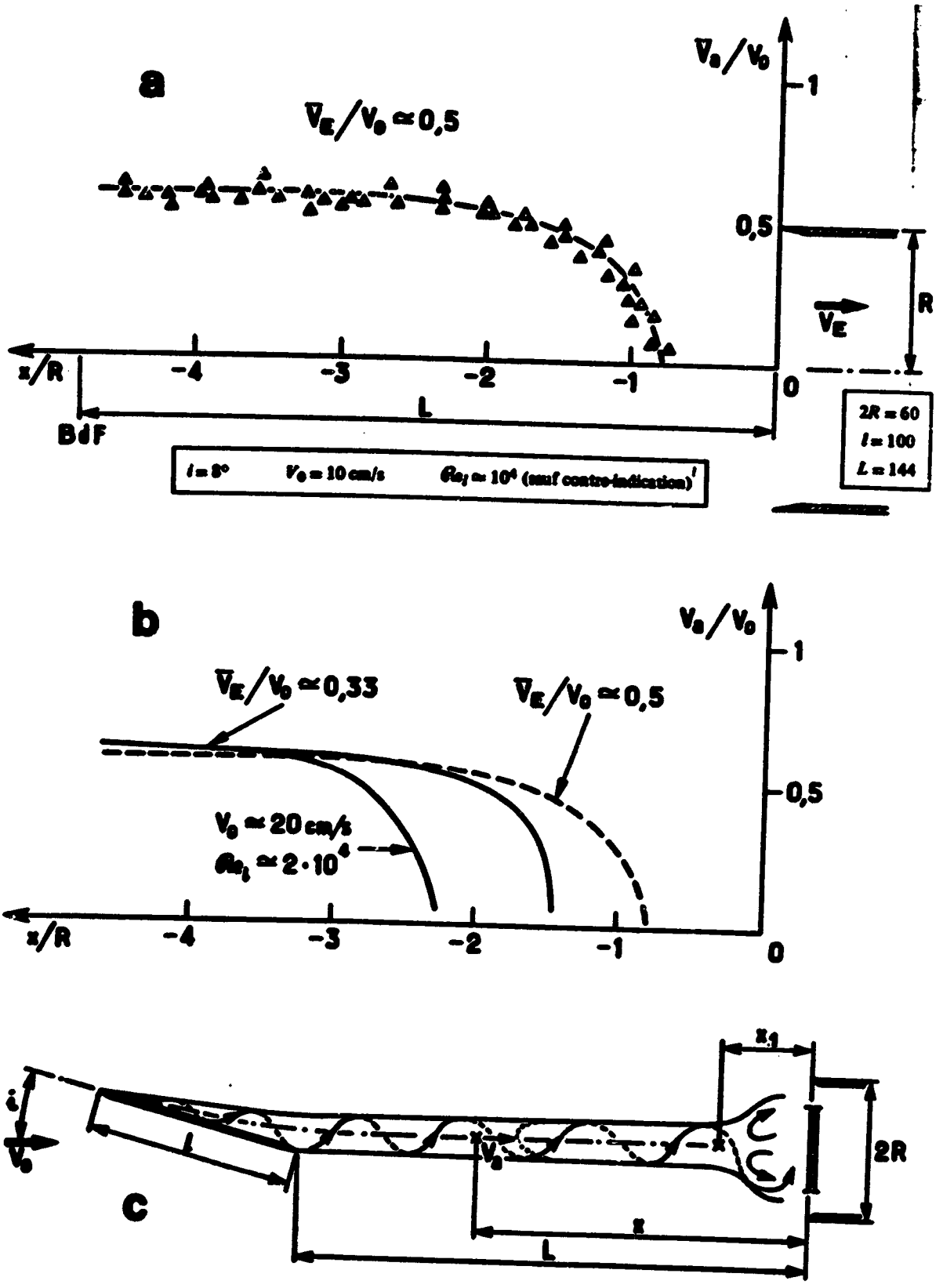

Figure 12. Evolution of the velocity along the vortex axis of the airfoil bursting before an air intake.

a) curve obtained for V_E/V_O=0.5 b) influence of the ratio of the velocities V_E/V_O and the velocity V_O (Re_l) c) diagram relative to the vortex nucleus

Key: 1-unless contra-indicated

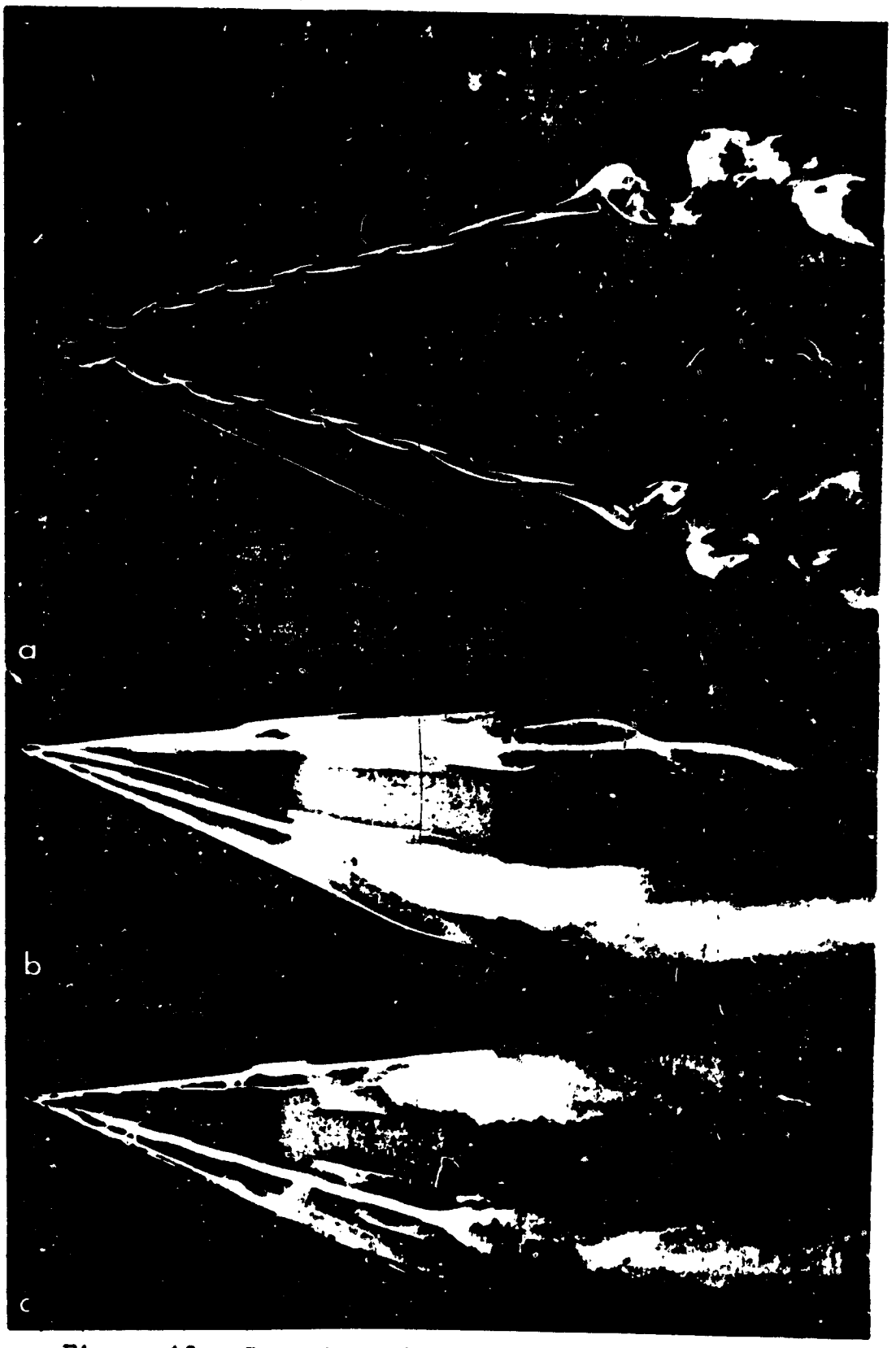

Figure 13. Bursting of vortices of apex of a Delta wing with incidence and without side-slipping.

a) natural bursting observed for $i=20^{o}$; $\varphi_{BA}=65^{o}$; $Re_{1a} \simeq 0.65 \cdot 10^{4}$; $l_a=130$
b) influence of downstream aspiration ($Q_A \simeq 13$ cm^3/s) } in the axis of one
c) influence of an obstacle placed downstream ($\phi 4$) } of the two vortices
$i=30^{o}$; $\varphi_{BA}=75^{o}$
$Re_{1a} \simeq 10^{4}$; $l_a=100$

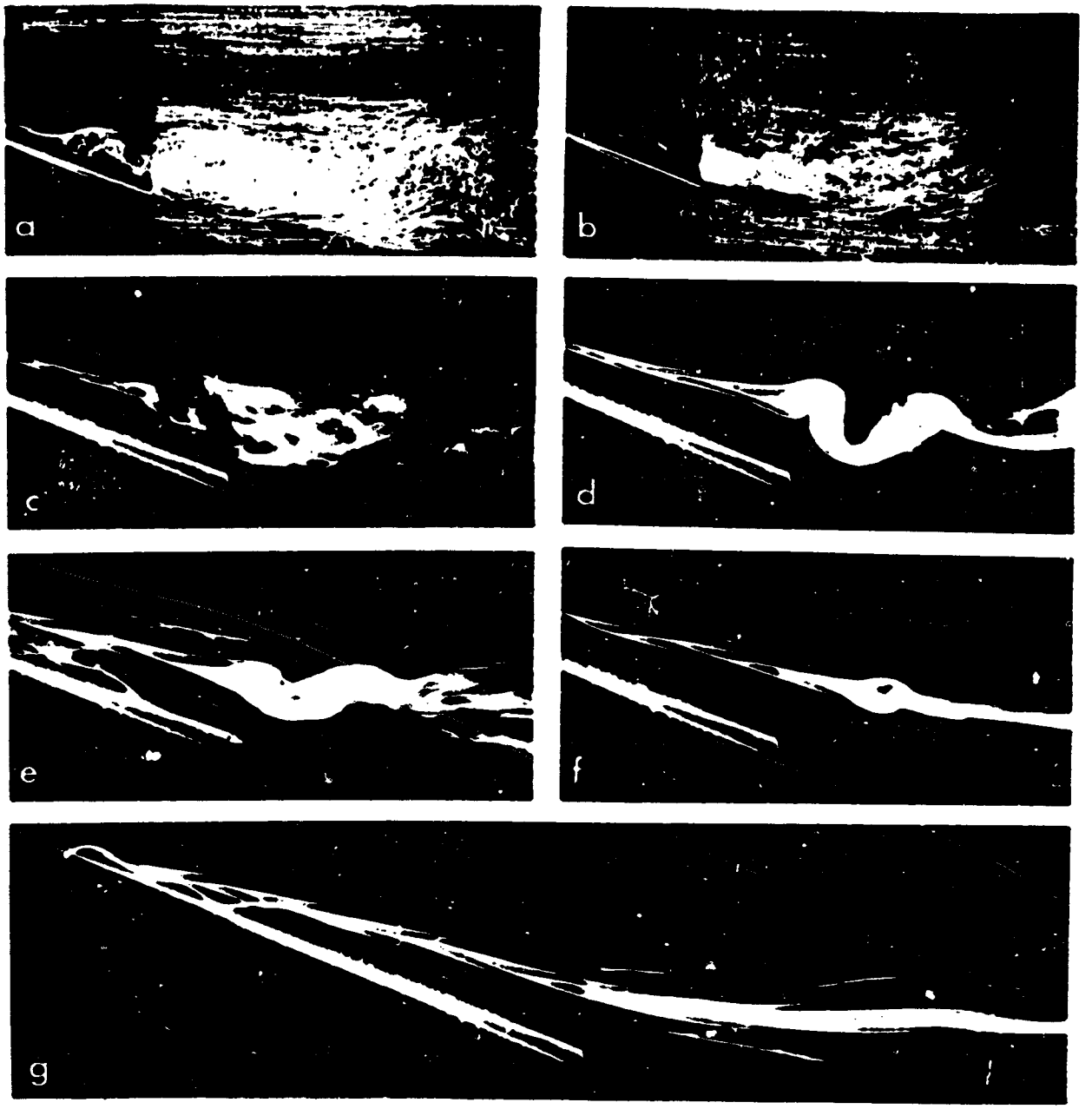

Figure 14. Types of burstings of vortices observed following the functional regime of an air intake arranged downstream of a thin Delta wing with incidence (rectangular air intake acting on the two vortices of the wing).

a) $V_E \simeq 0.5\ V_o$ premature bursting
b) $V_E \simeq 0.9\ V_o$
c) $V_E \simeq V_o$ pseudo-natural bursting
d) $V_E \simeq 2^o V_o$ delayed bursting

} around an indefinite separated pocket and with mixed character (Re_1 from $0.5 \cdot 10^4$ to 10^4)

e) $V_E \simeq 3V_o$
f) $V_E \simeq 4V_o$

} delayed bursting around the finite separated pocket and with mixed character

{ mixed character $Re_1 \simeq 0.5 \cdot 10^4$ entirely laminar $Re_1 \simeq 0.25 \cdot 10^4$

g) $V_E \simeq 6V_o$ resorbed bursting ($Re_1 \simeq 0.25 \cdot 10^4$)

visualization by air bubbles (a and b) of flow in longitudinal plane pasing through vortex axis situated to left side of the airfoil; visualizaiton of vortex by colored emission (c, d, e, f, and g) $i=20^o$; $j=0^o$; $\varphi_{BA}=65^o$; $l=100$

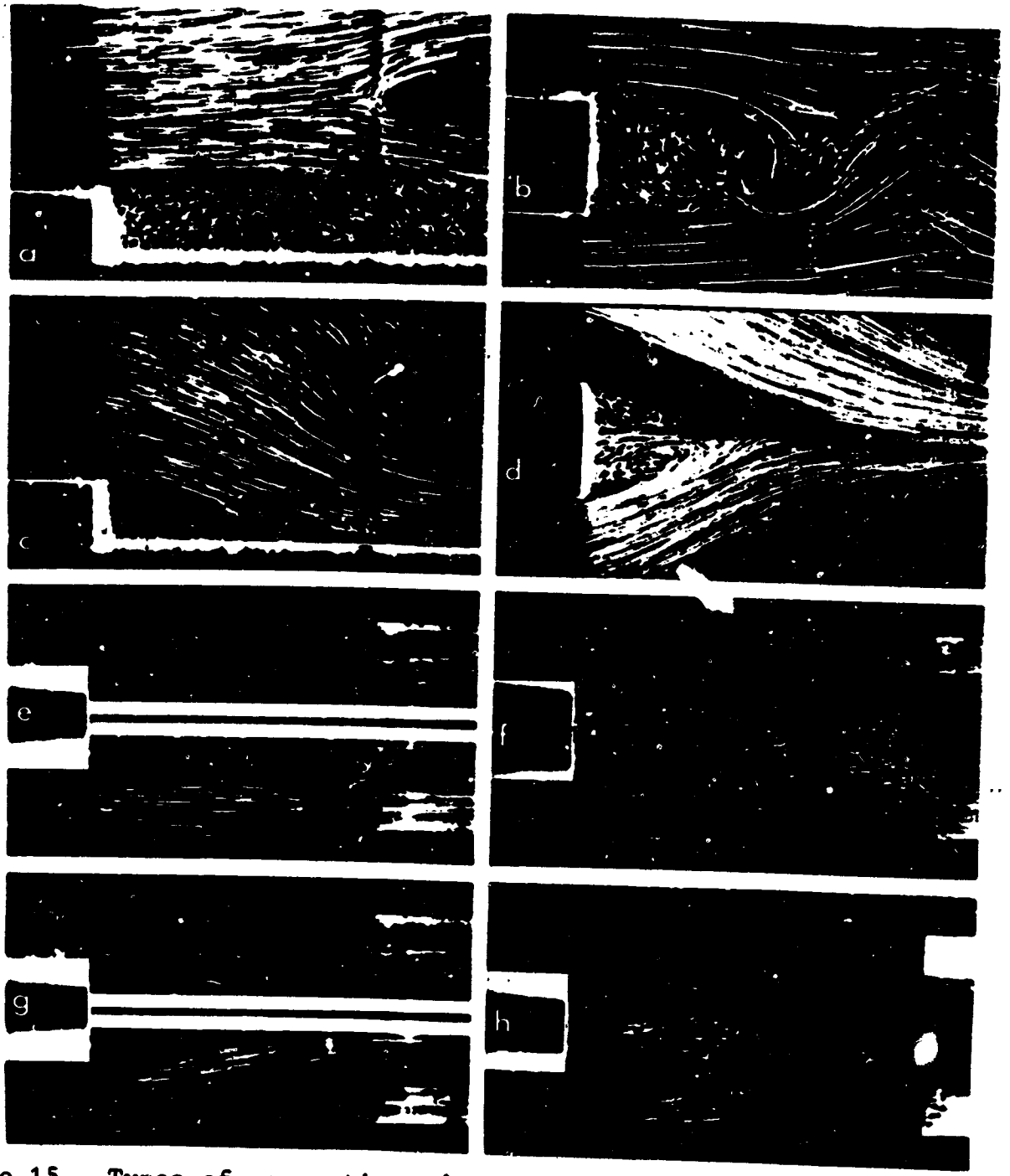

Figure 15. Types of separations downstream of wall stalling (a, c, e, and g) and wakes behind a straight base (b, d, f and h) observed following the functional regime of a downstream air intake.

a) indefinite separated zone: $V_E \simeq \varepsilon V_o$; $Re_1 \simeq 2 \cdot 10^4$
c) finite separated zone: $V_E \simeq 10\varepsilon V_o$; $Re_1 \simeq 0.5 \cdot 10^4$
b) indefinite wake: test without downstream air intake $Re_1 \simeq 10^4$
d) finite wake: $V_E \simeq 10\varepsilon V_o$; $Re_1 \simeq 0.1 \cdot 10^4$

} tests in planar current (views of the plane of symmetry)

e) indefinite separated zone: $V_E \simeq 0.75\varepsilon V_o$; $Re_1 \simeq 2 \cdot 10^4$
g) finite separated zone: $V_E \simeq 6\varepsilon V_o$; $Re_1 \simeq 10^4$
f) indefinite wake: $V_E \simeq 0.2\varepsilon V_o$; $Re_1 \simeq 4 \cdot 10^4$
h) finite wake: $V_E \simeq 10\varepsilon V_o$; $Re_1 \simeq 0.5 \cdot 10^4$

} tests in rotational flow (views in diametral plane)

$\varepsilon = \frac{S_P - S_D}{S_P}$ with $\begin{cases} S_P = \text{surface of the section of the air intake entry} \\ S_D = \text{surface of the separation or straight base} \end{cases}$

height of the stall or base: from 10 to 30
air intake-stall or base distance: L from 65 to 110 } according to case

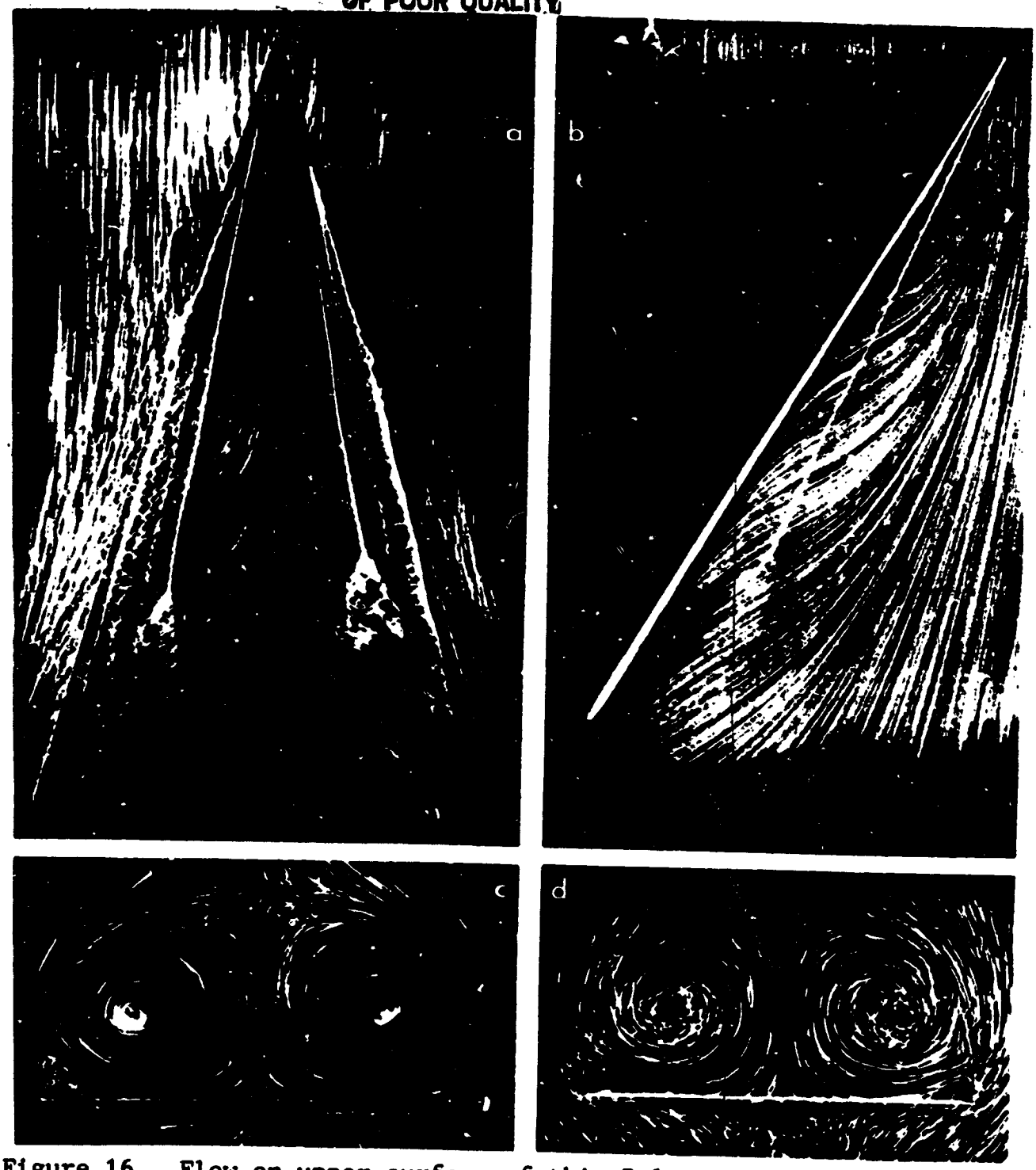

/32

Figure 16. Flow on upper surface of thin Delta wing at high incidences

a) flow in the vicinity of the upper surface
b) flow in the plane of symmetry
c) flow in transversal plane situated at mid-chord } axis of intakes
d) flow in transversal plane situated at flight edge } from views parallel to wing axis

$\varphi_{BA}=75^{o}$; $j=0$; $I_a=200$; Re_{1a} from $2 \cdot 10^4$ to $4 \cdot 10^4$; $i_{geometric}=30^{o}$ with $i_{effective}=32.6^{o}$ after correction for the obstruction effect (see figure 20)
(unless contra-indicated)
visualization by air bubbles

/33

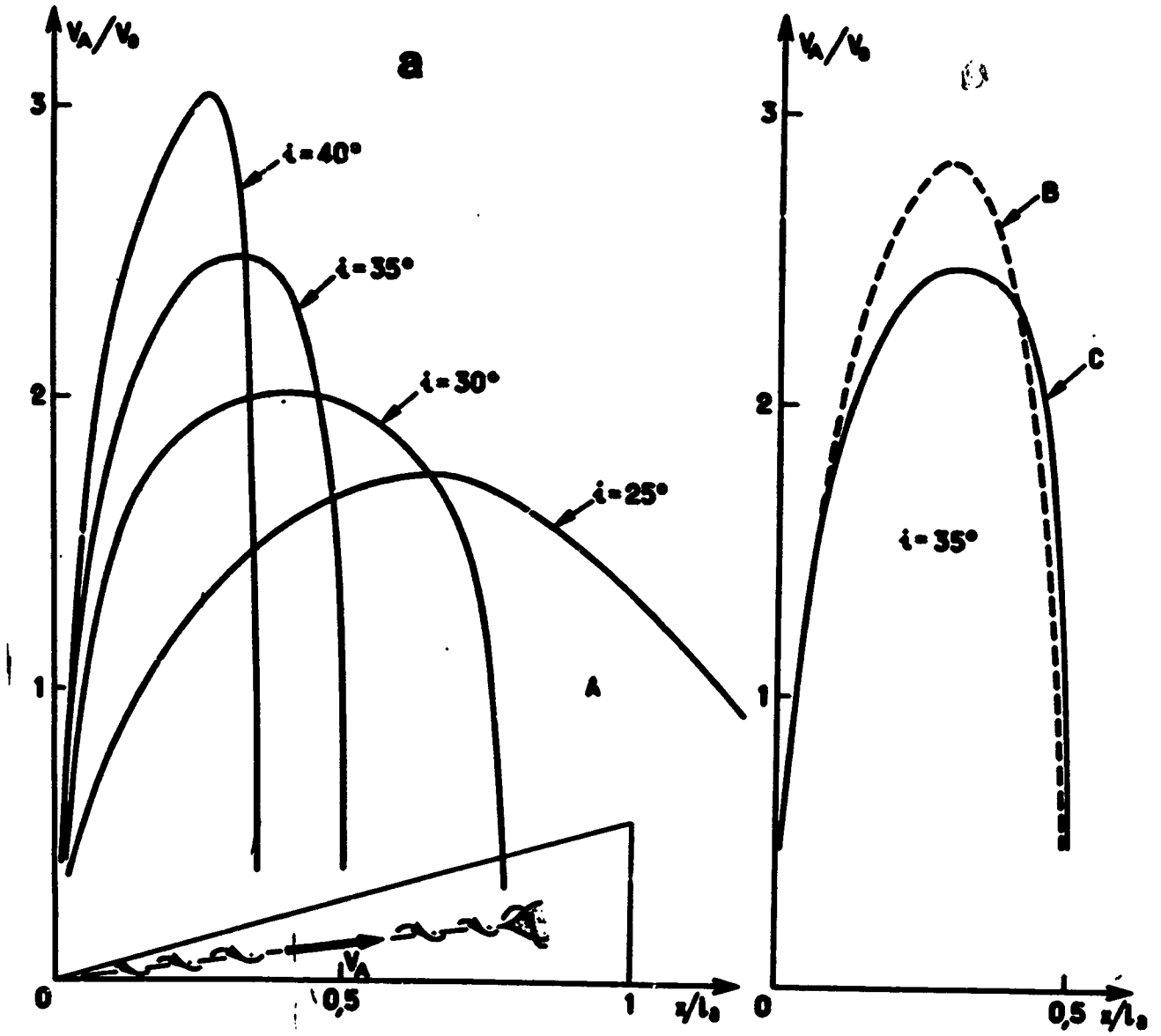

Figure 17. Evolution of velocity along vortex axis of Delta wing with incidence.

a) influence of incidence
b) influence of velocity (Re_{l_a})

Thin Delta wing with sharp edges: $\varphi_{BA}=75^{\circ}$; $\lambda=1.07$; $j=0$; $e/l_a=1\%$; $l_a=200$

A: $V_o=10$ cm/s $Re_{l_a} \simeq 2 \cdot 10^4$

B: $V_o=20$ cm/s $Re_{l_a} \simeq 4 \cdot 10^4$

C: $V_o=10$ cm/s $Re_{l_a} \simeq 2 \cdot 10^4$

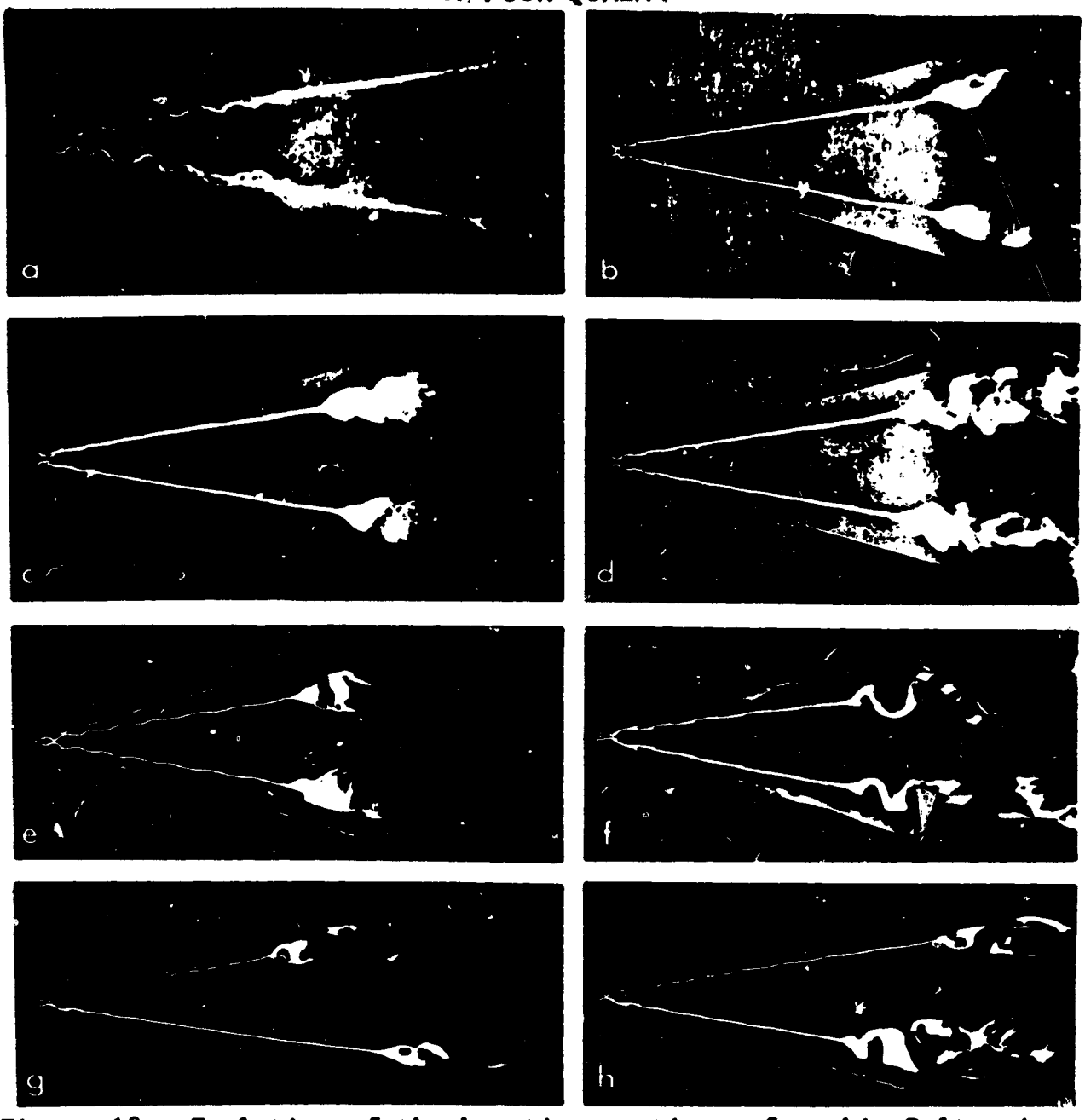

/34

Figure 18. Evolution of the bursting vortices of a thin Delta wing at high incidences as a function of the Reynolds number Re_{1a}

a. $Re_{1a} \simeq 5{,}3 \cdot 10^6$ } $l_a = 320$
b. $Re_{1a} \simeq 4 \cdot 10^6$
c. $Re_{1a} \simeq 3 \cdot 10^6$ } $l_a = 200$
d. $Re_{1a} \simeq 2 \cdot 10^6$
e. $Re_{1a} \simeq 10^6$
f. $Re_{1a} \simeq 0{,}5 \cdot 10^6$ } $l_a = 100$
g. $Re_{1a} \simeq 10^6$
h. $Re_{1a} \simeq 10^6$

$i = 30^o$; $j = 0^o$; $\varphi_{BA} = 75^o$
for a, it is taken into account from the significant obstruction effect (geometric incidence $i = 24^o$)
thin wings with sharp bevelled upper surface side edges and for $l_a \geq 200$ and symmetrically for $l_a = 100$

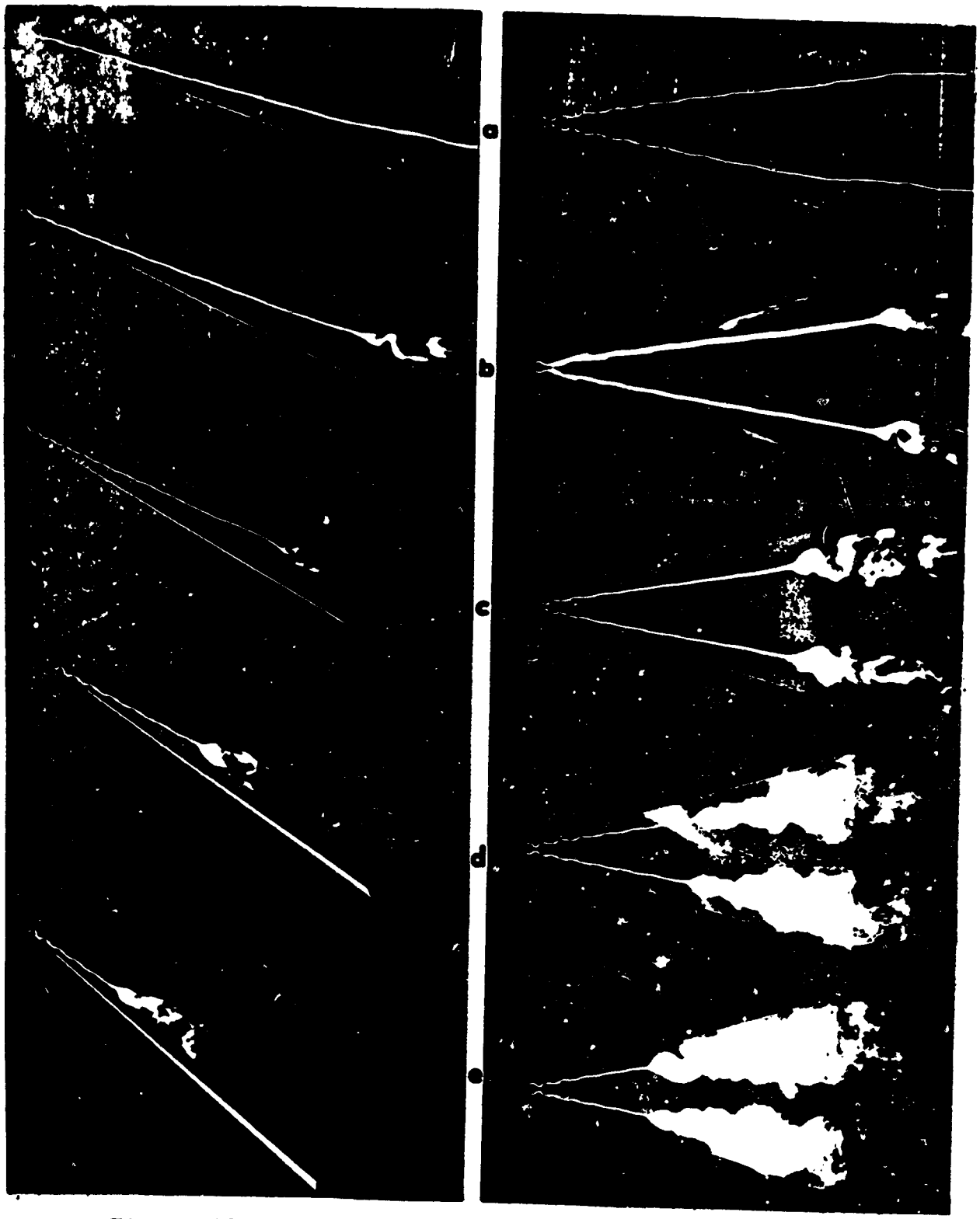

Figure 19. Evolution of the bursting of vortices of a thin Delta wing as a function of incidence.

a. $i_o = 20°$ $i_{eff} = 21°,6$
b. $i_o = 25°$ $i_{eff} = 27°,2$
c. $i_o = 30°$ $i_{eff} = 32°,6$
d. $i_o = 35°$ $i_{eff} = 37°,85$
e. $i_o = 40°$ $i_{eff} = 42°,6$

$\varphi_{BA}=75^o$; $j=0^o$; $l_a=200$; $Re_{l_a} \simeq 2 \cdot 10^4$
i_o=geometric incidence; i_{eff}=effective incidence with correction for the obstruction effect
at left, views of the outline; at right, views of upper surface
visualization by colored emissions

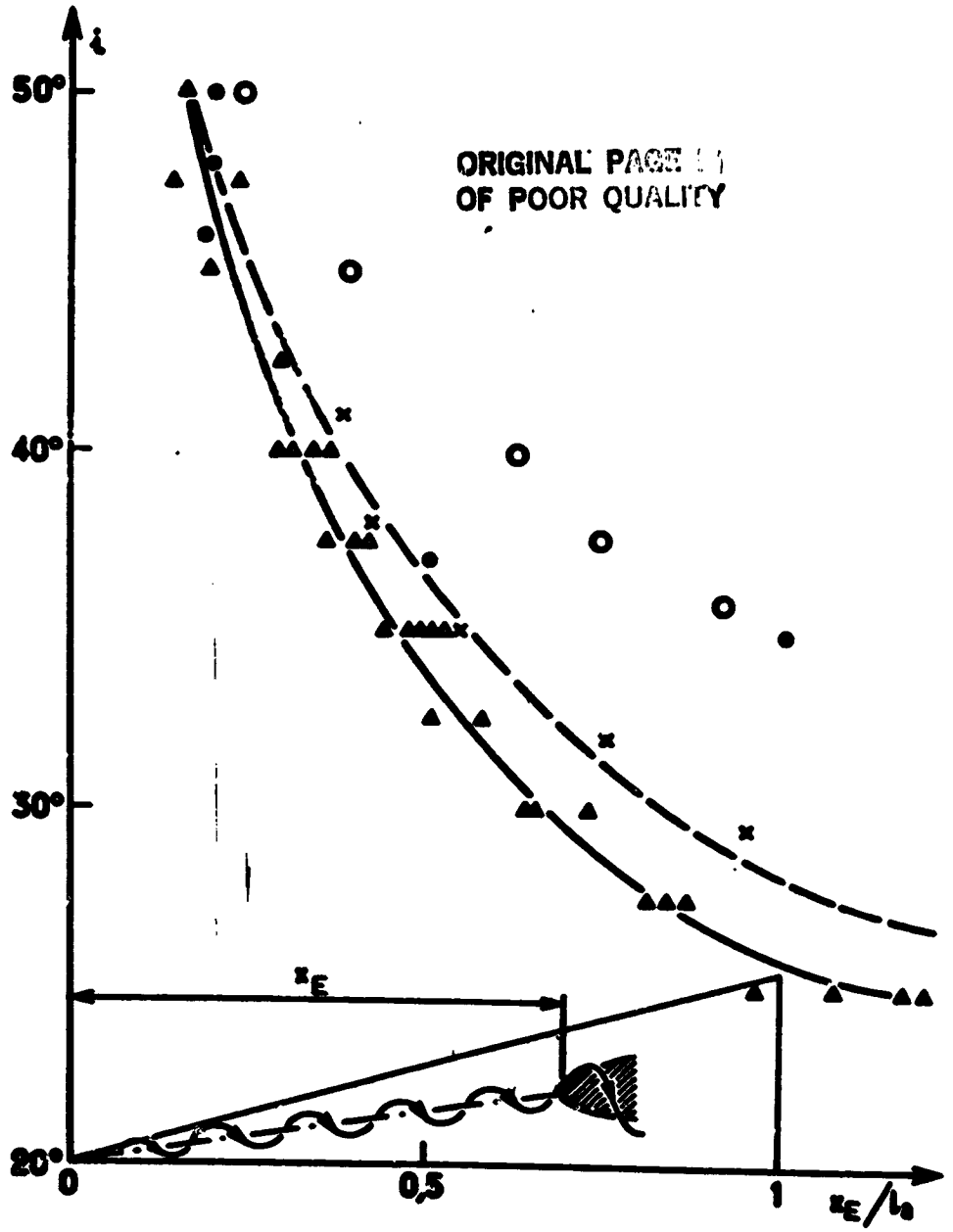

Figure 20. Displacement of the bursting point of the vortices of a thin Delta wing as a function of the incidence. Comparison between the results obtained with the hydrodynamic tunnel and those of measurements carried out in wind tunnels.

Thin Delta wing with sharp edges: $\varphi_{BA}=75^o$; $\lambda=1.07$; $j=0^o$; $l_a=200$
Tests with ONERA hydrodynamic tunnel
Δ without } correction for the obstruction effect (V_o from 10 to 20
---with } cm/s; Re_{l_a} from $2\cdot10^4$ to $4\cdot10^4$)
× after D. Hummel [26] ($\lambda=1$; $l_a=750$; $Re_{l_a}\simeq 2\cdot10^6$)
● after W. Wentz and D. Kohlman [49] ($\lambda=1.07$; $l_a=457$; $Re_{l_a}\simeq 10^6$
○ after P. Earnshaw and J. Lawford [11] ($\lambda=1$; $l_a=2$[illegible]; Re_{l_a} from $0.4\cdot10^6$ to $0.9\cdot10^6$)

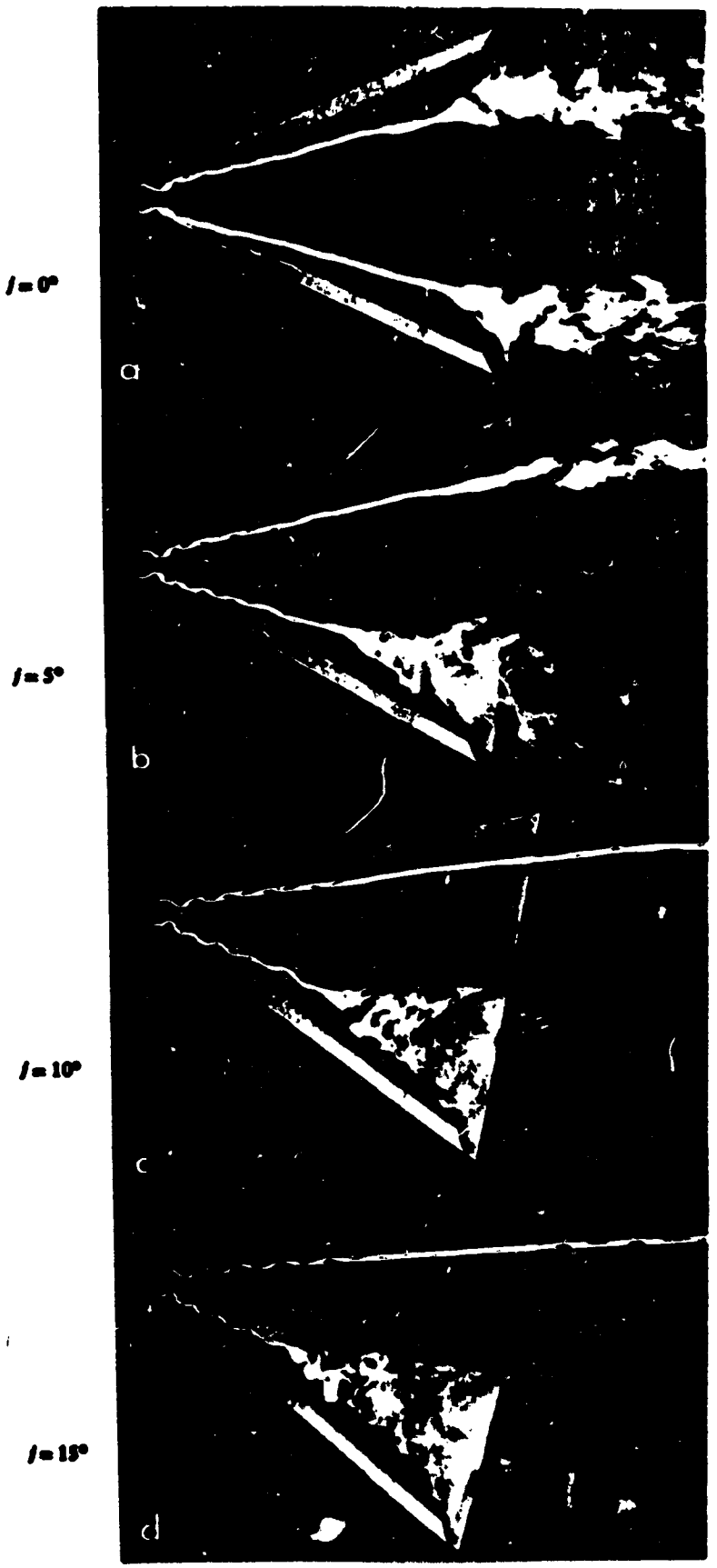

Figure 21. Evolution of the bursting of vortices of a thin Delta wing with incidence as a function of side-slipping.

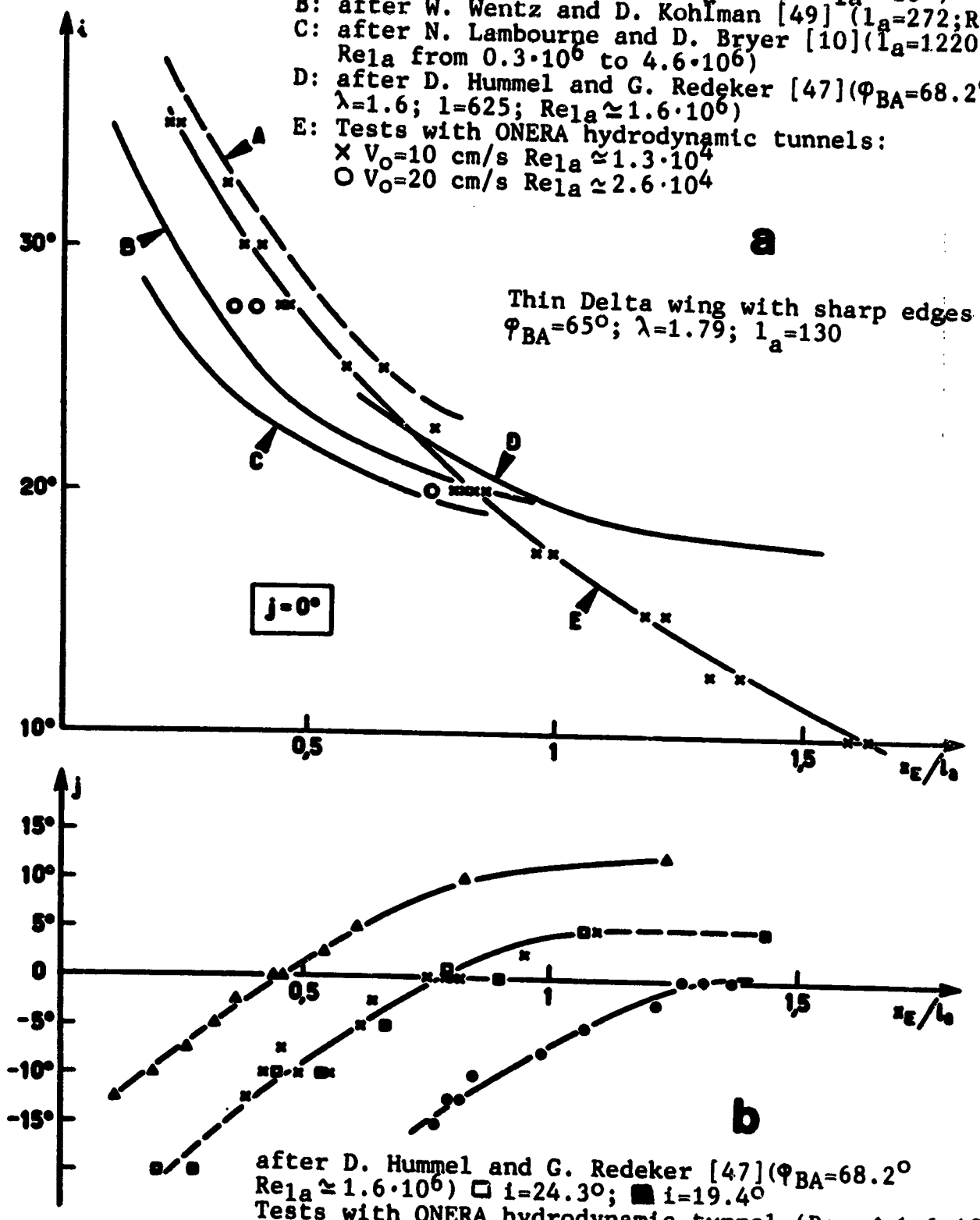

Figure 22. Displacement of the bursting point of vortices of a thin Delta wing as a function of incidence and side-slipping.
a) influence of incidence
b) influence of side-slipping
} comparisons between the results obtained with hydrodynamic tunnels and those of measurements in wind tunnels

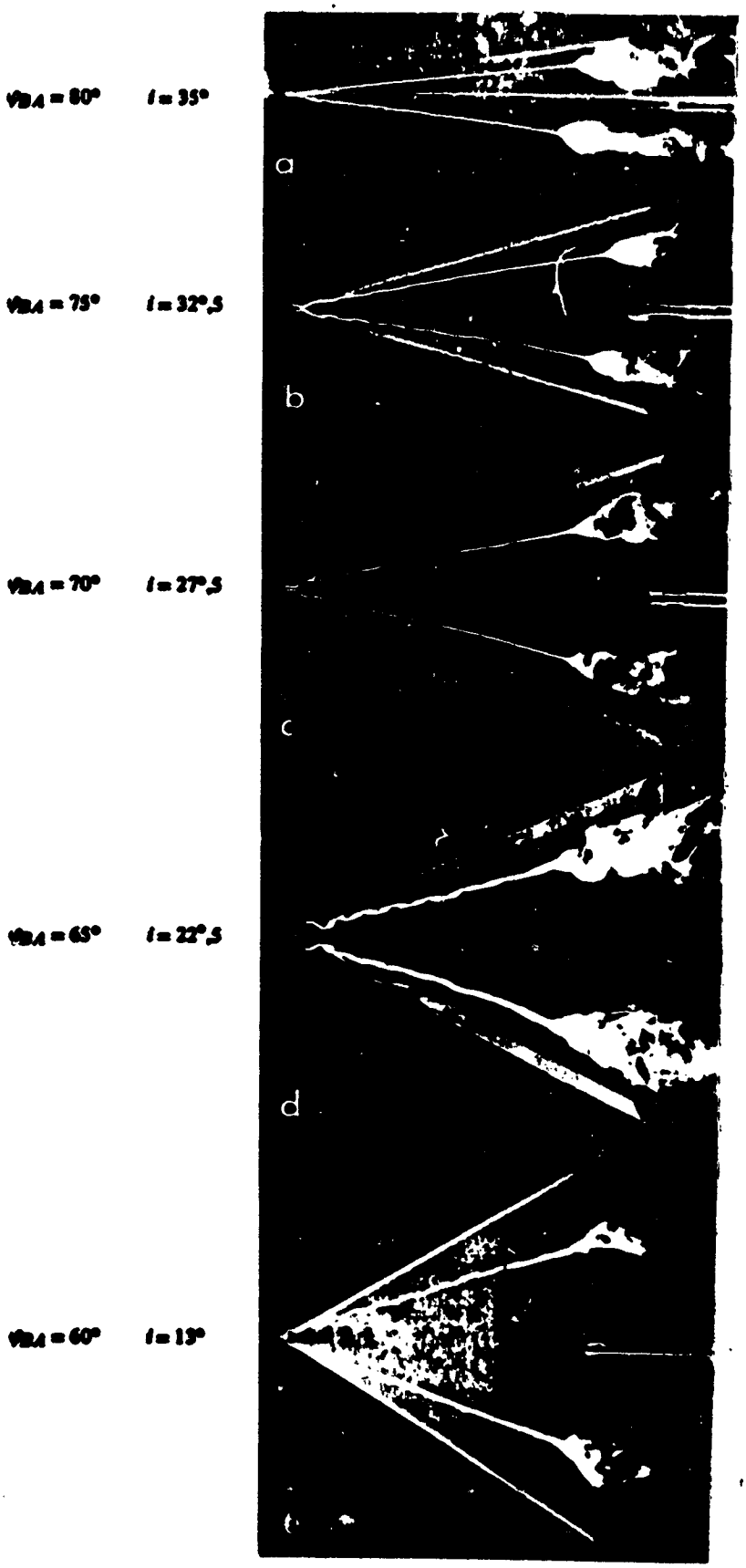

Wing with edges bevelled symmetrically $j=0^{o}$; $l_a=100$; $Re_{l_a} \simeq 10^4$ (except for d, $l_a=130$; $Re_{l_a} \simeq 1.3 \cdot 10^4$)

Figure 23. Evolution of the bursting of vortices of a thin Delta wing as a function of the leading flight edge.

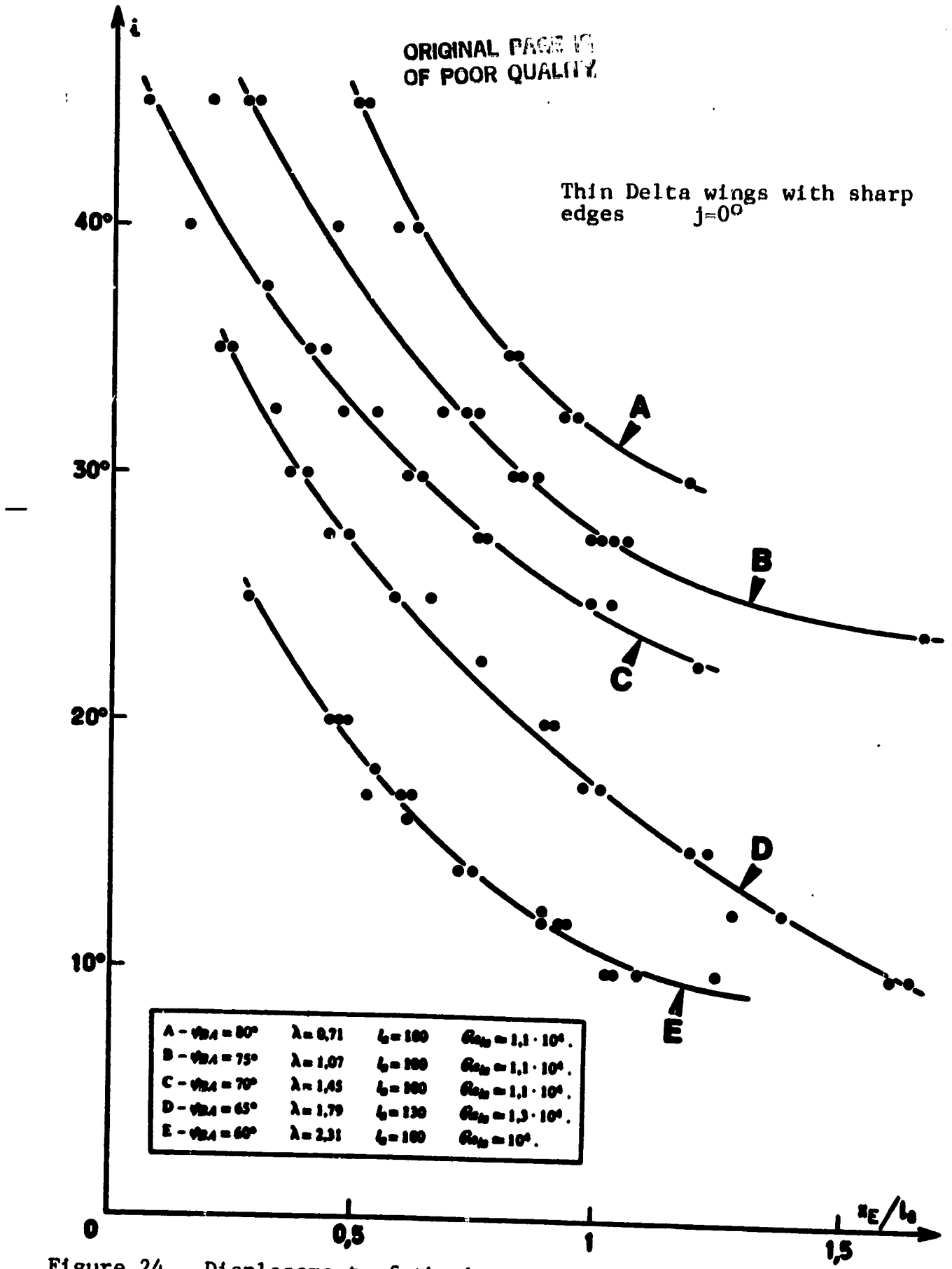

Figure 24. Displacement of the bursting point of vortices of a thin Delta wing as a function of the incidence. Comparison between the curves obtained for different airfoils whose leading edge varies between 80° and 60°.

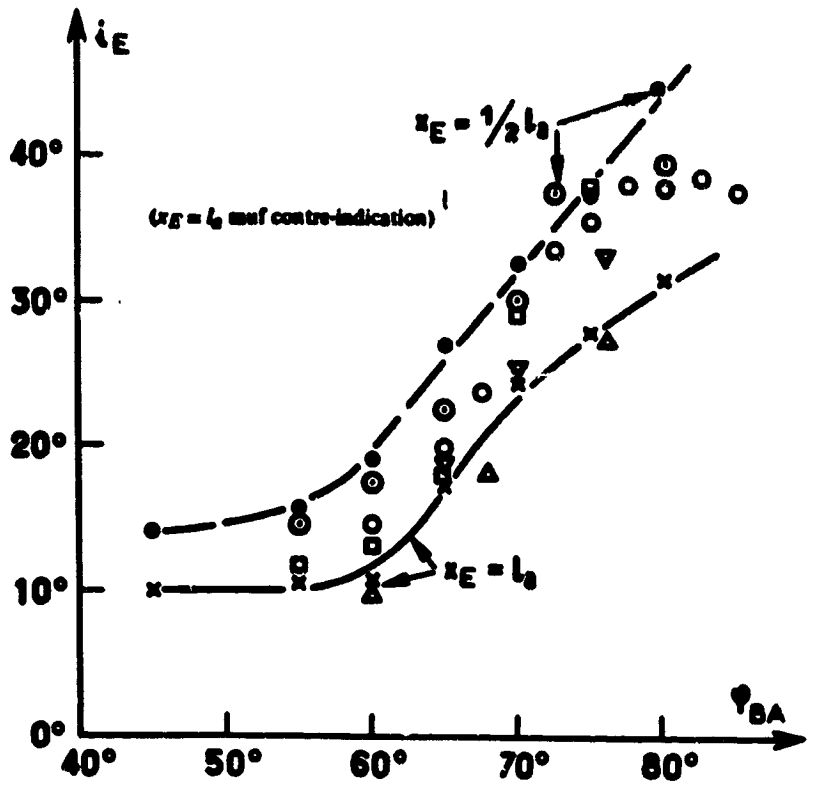

Figure 25. Influence of the leading flight edges on the incidence i_E for which the bursting of vortices of a thin Delta wing is produced on the flight edge (or at the mid-chord).

Comparison between the results obtained with hydrodynamic tunnels and those of measurements carried out in wind tunnels.

● × Tests with ONERA hydrodynamic tunnel ($Re_{la} \simeq 10^4$)

Wind tunnel tests ($Re_{la} \simeq 10^6$):
- □ after Ph. Poisson-Quinton and E. Erlich [25]
- ⊙ ○ after W. Wentz and D. Kohlman [49]
- △ after D. Hummel and P. Srinivassan [39]
- ▽ after P. Earnshaw and J. Lawford [11]

Key: 1-($X_E = l_a$ unless contra-indicated)

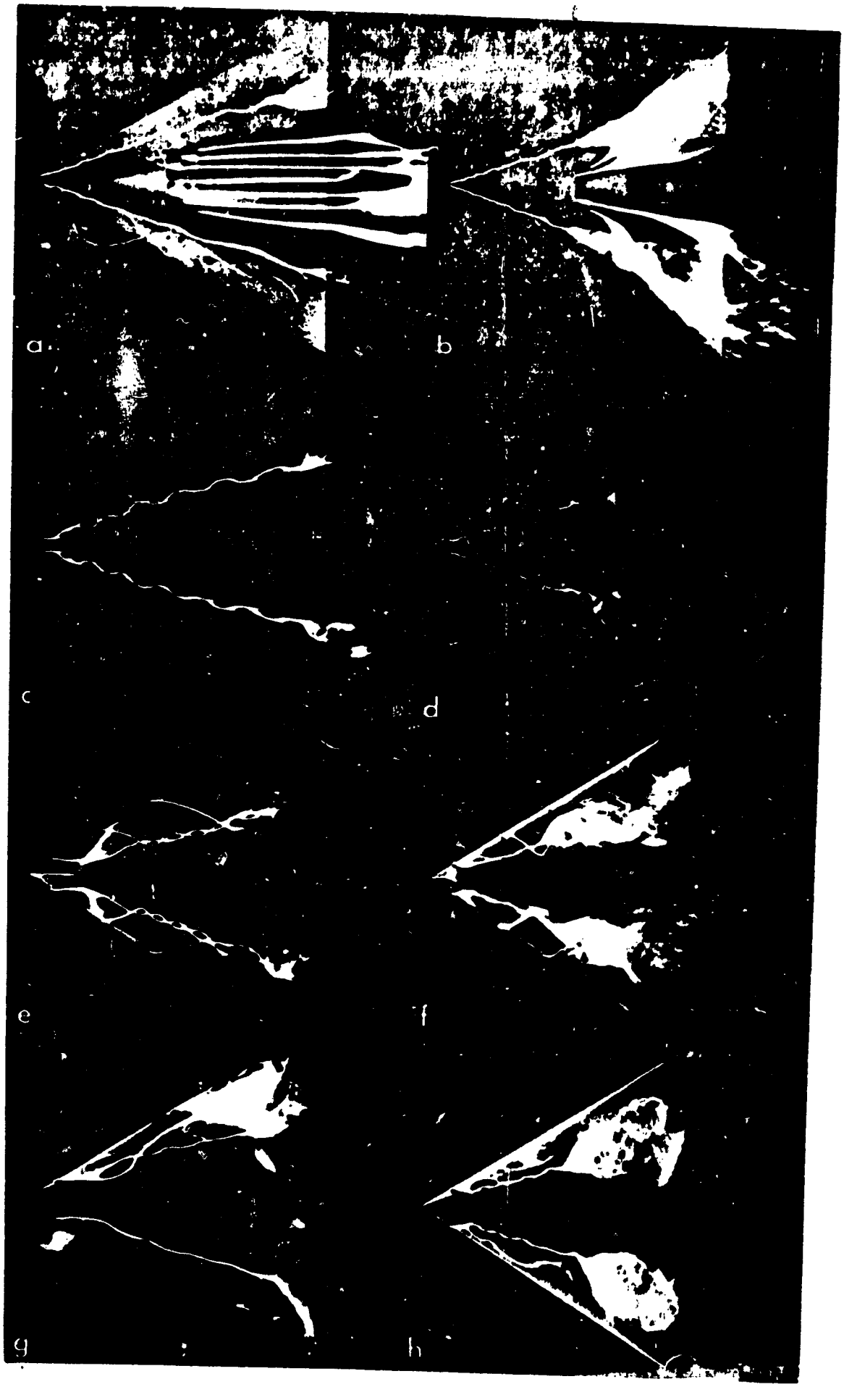

see facing page

Figure 26. Influence of the thickness and form of the shape, particularly with the leading edge on the bursting of vortices of a Delta wing.

a) $i=8^{o}$ } shape of plate types with bevelled edges
b) $i=16^{o}$ } upper surface side ($e/l_a=1\%$)
c) $i=12^{o}$ } shape of plate type with bevelled edges
d) $i=20^{o}$ } symmetrical ($e/l_a=1\%$)
e) $i=15^{o}$ } shape of plate type with curved edges
f) $i=24^{o}$ } (symmetrical shape with stopping of leading edge $e/l_a=5\%$)
g) $i=16^{o}$ } shape following the plane of symmetry constituted by two
h) $i=25^{o}$ } arcs of a circle and transversal elliptical shapes ($e/l_a=10\%$)

$\varphi_{BA}=60^{o}$; $j=0^{o}$; $l_a=100$; $Re_{l_a} \simeq 10^{4}$

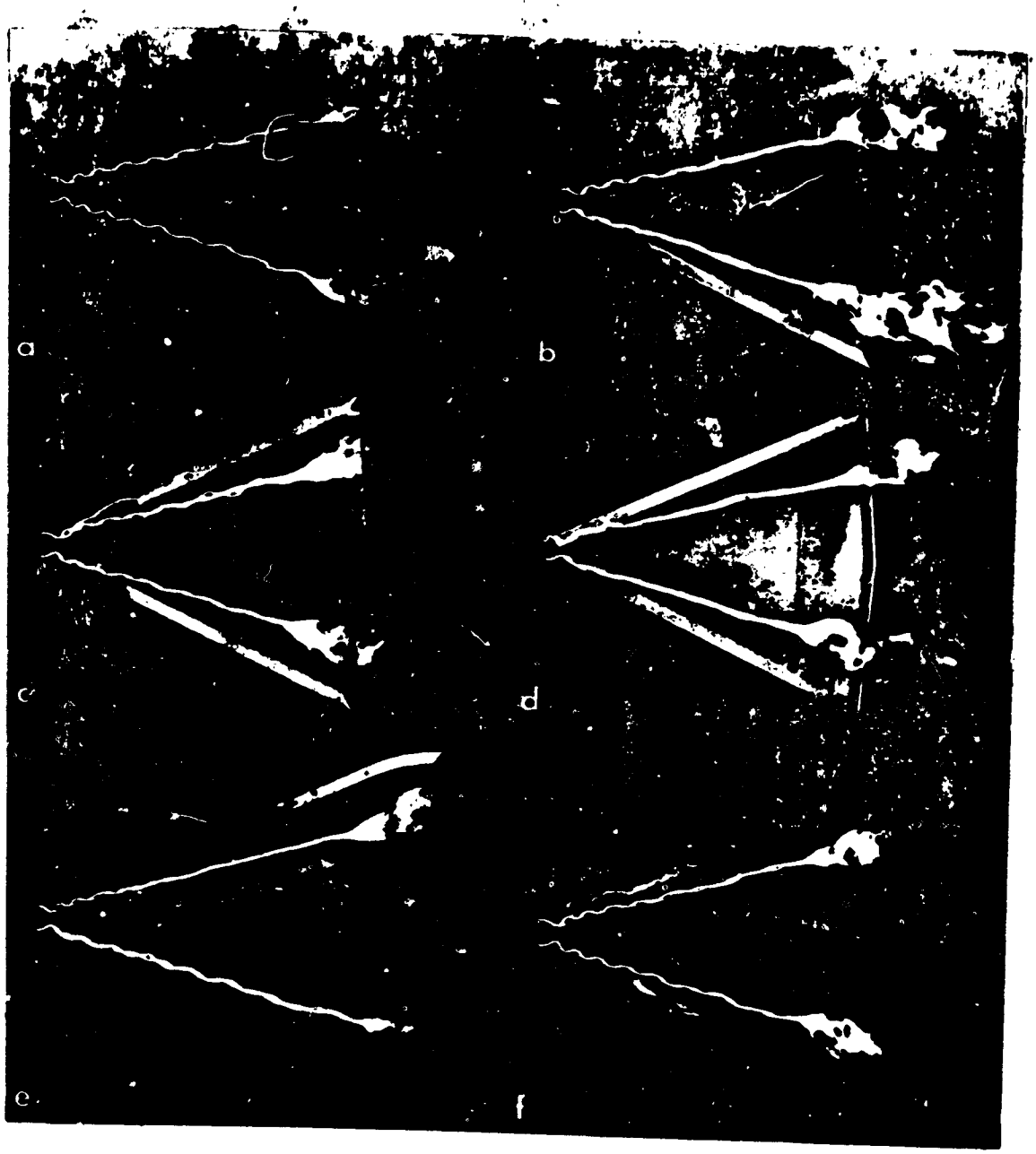

Figure 27. Influence of the planar form of the rear end on the bursting of vortices of a thin Delta wing with incidence.

a) old fashioned Delta wing
b) Delta wing ($\varphi_{BdF}=0^o$)
c) Delta wing
d) Delta wing with straight-sided flight edge strip
e) old fashioned Delta wing (large model)
f) double-flight Delta wing ($\varphi_{BA}=45^o$ near BdF)

Models of plate type (e=2) with bevelled symmetrical edges)
$i=20^o$; $j=0^o$; $\varphi_{BA}=65^o$; $\varphi_{BdF}=-5^o$ (unless contra-indicated);
$l_a=130$ $Re_{la} \simeq 1.3 \cdot 10^4$ for a, b, c, d and f
$l_a=170$ $Re_{la} \simeq 1.7 \cdot 10^4$ for e

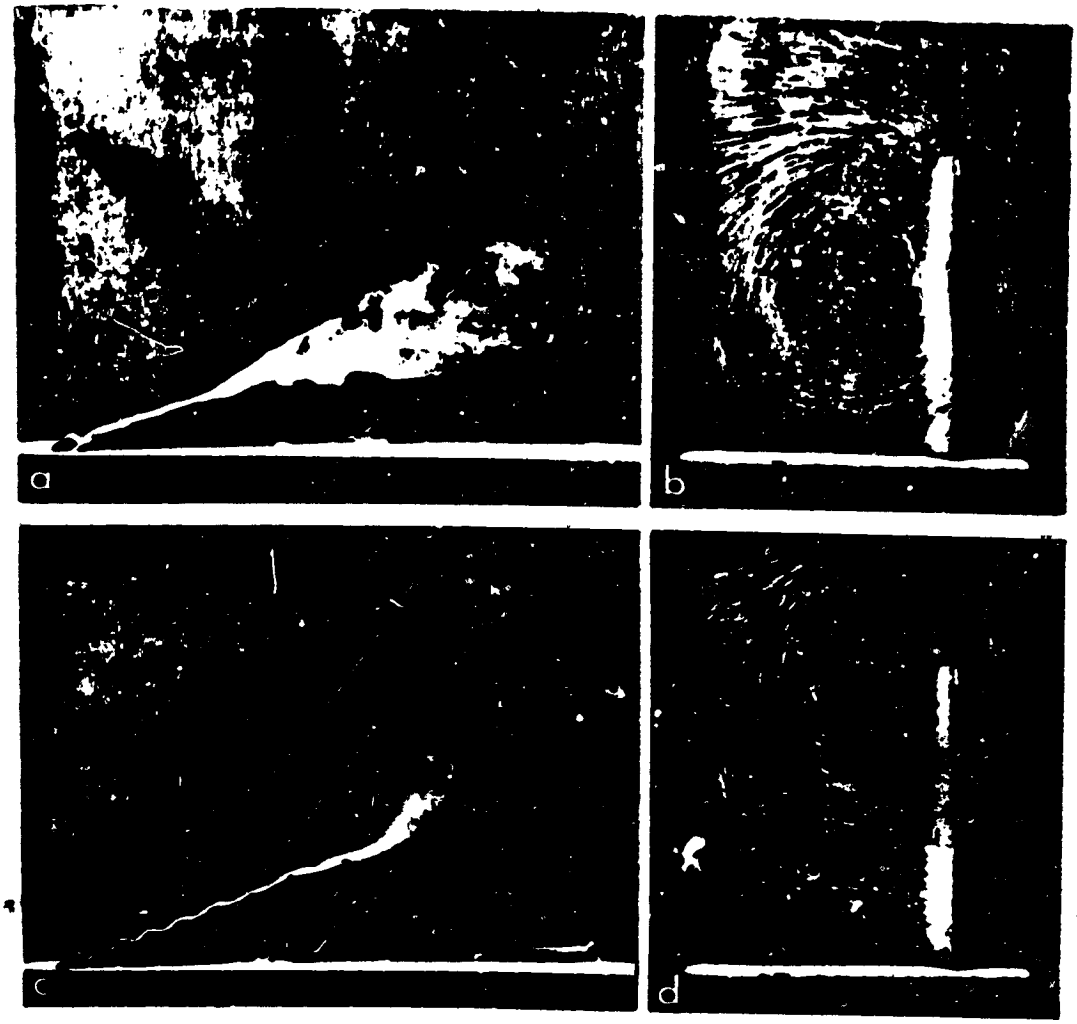

Figure 28. Influence of a jet emitted following the vortex axis on the bursting around a thin Delta wing with incidence.

a) view of the upper surface
b) flow in a transversal plane situated in the vicinity of the flight edge
} test without jet

c) view of the upper surface
d) flow in a transversal plane situated in the vicinity of the flight edge
} test with jet (ϕ_{jet} 1.5-blast carried out at the mid-chord) $c_\mu \simeq 0.5$ ($\bar{V}_j \simeq 30V_o$)

1/2 model mounted to the wall $i=25^o$
plate (e=2) with bevelled upper surface side edges
$\varphi_{BA}=60^o$; tapering=0.1; $l_a=150$; $Re_{la} \simeq 1.5 \cdot 10^4$

see facing page

Figure 29. Bursting of vortices on airplane models with flight wings and with simulation of the jet engines.

a) view of the upper surface
b) flow in a transversal plane situated in the vicinity of the flight edge

} "Concorde" type airplane with incidence and side-slipping 1/140 model; chord on the airplane axis l_a=225; i=12°; j=10°; $Re_{l_a} \simeq 2 \cdot 10^4$

d) view of the outline (upper surface side
f) perspective view form the rear

} Douglas F5D airplane with ogival wing 1/72.5 model; mean chord $\bar{l}$=95 i=15°; j=0°; $Re_{\bar{l}} \simeq 10^4$

c) perspective view (upper surface side
e) perspective view from the rear

} flight test of Douglas F5D [31] images extracted from NASA film [66]

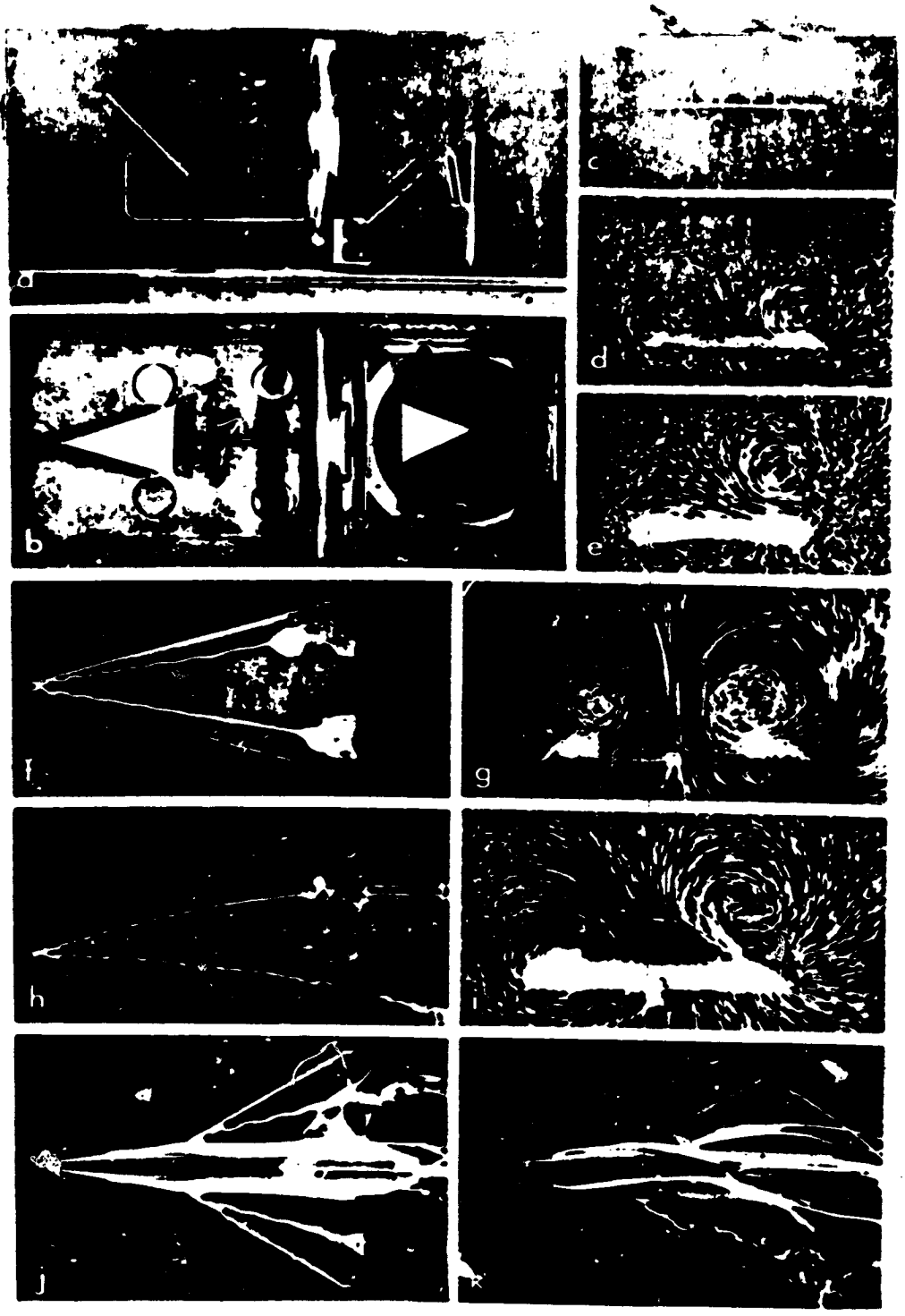

Figure 30. Bursting of vortices on thin Delta wings propelled by uniform rotational movement. Views of upper surface (f, h, j and k) and flow in a transversal plane situated in the vicinity of the flight edge (c, d, e, g and i).

a) and b) views of test mounting adopted

c, incidence $i = 0°$ $N = 0,6$ tr/s $\frac{\omega b}{V_0} = 0,45$

d, e, incidence $i = 15°$ { $N = 0$ / $N = 0,4$ tr/s } $\frac{\omega b}{V_0} = 0,30$

f, g, h, i, incidence $i = 30°$ { $N = 0$ / $N = 0,2$ tr/s } $\frac{\omega b}{V_0} = 0,15$

Delta wing with sharp edges $\varphi_{BA}=75°$; $j=0°$; $l_a=100$; $Re_{l_a} \simeq 1.1\ 10^4$ b=1/2 wingspan; rotation axis passing through the middle of the wing

j, k, incidence $i = 15°$ { $N = 0$ / $N = 0,2$ tr/s } $\frac{\omega b}{V_0} = 0,21$

airplane equipped with Delta wing with sharp edges; $\varphi_{BA}=60°$; $j=0°$; $l_a=69$; $Re_{l_a} \simeq 0.75 \cdot 10^4$; rotation axis 75% l_a

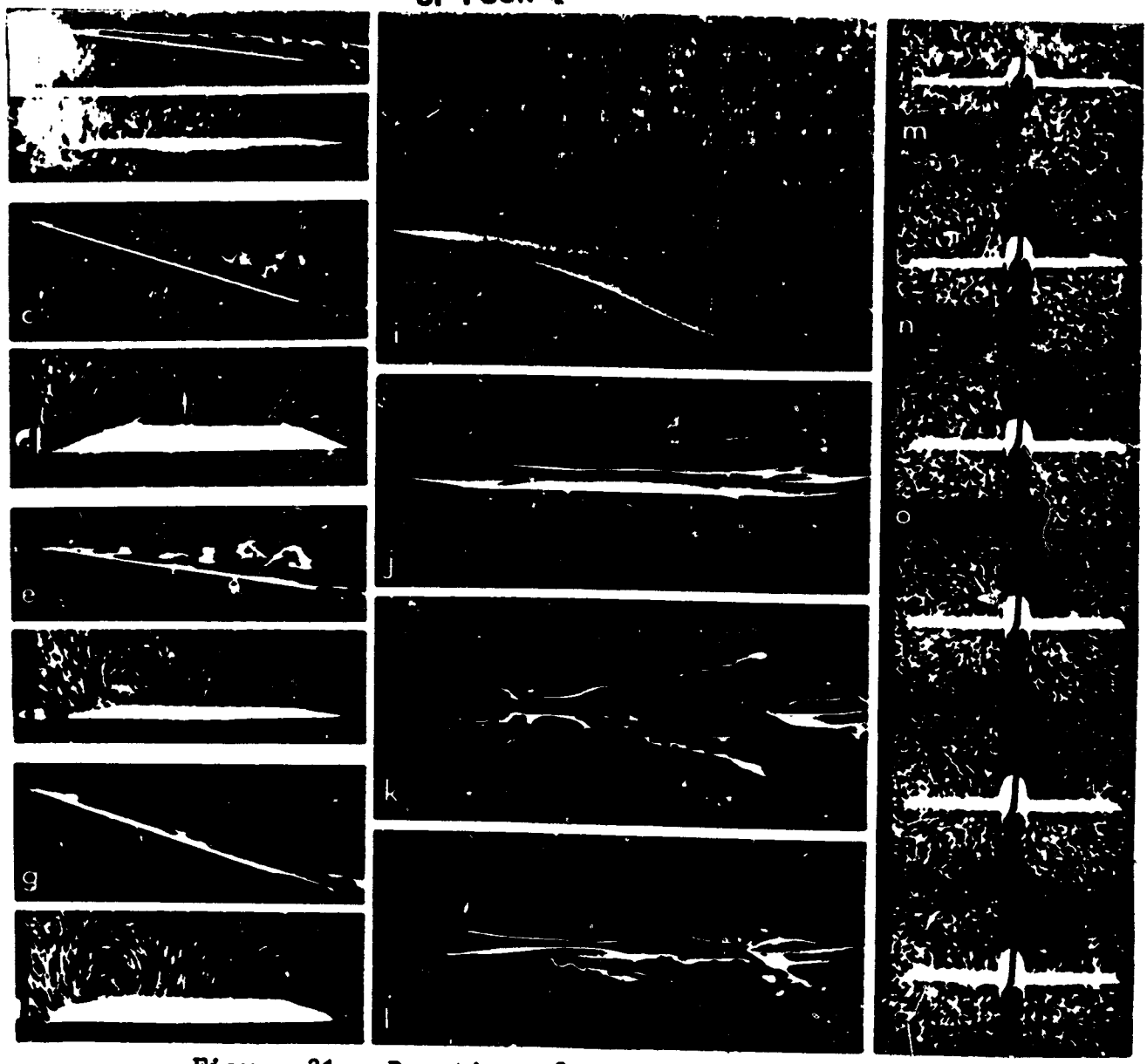

Figure 31. Bursting of vortices on thin Delta wings propelled by periodic pitching oscillations.

i) view of test mounting adopted (law of sinusoidal incidence; mean incidence $\bar{i}=12^o$; amplitude $i=\pm 5^o$)

a) and b) $\bar{i}=7^o$ } fixed model
c) and d) $\bar{i}=17^o$ } (N=0)
e) and f) passage through $\bar{i}_{min}$ } oscillating model
g) and h) passage through $\bar{i}_{max}$ } (N=1 hertz)
j) $\bar{i}=12^o$ fixed model (N=0)

Delta wing with sharp edges: $\varphi_{BA}=60^o$ $j=0^o$; $l_a=100$; $Re_{l_a}\simeq 10^4$ pitching axis at 50% l_a

k) passage through $\bar{i}_{min}$
l) passage through $\bar{i}_{max}$
m) passage through $\bar{i}_{min}$
to r) passage through $\bar{i}_{max}$
} oscillating model (N=1 hertz)

"Concorde" type airplane (1/280 model without jet engine) $l_a=112$; $Re_{l_a}\simeq 1.2\cdot 10^4$ $j=0^o$; pitching axis situated at mid-chord

views of the outline (a, c, e, and g); views of the upper surface (j, k and l); views of the flow in a transversal plane situated in the vicinity : {of the mid-chord (b, d, f and h) / of the flight edge (m, n, o, p, q and r): successive images extracted from a test film

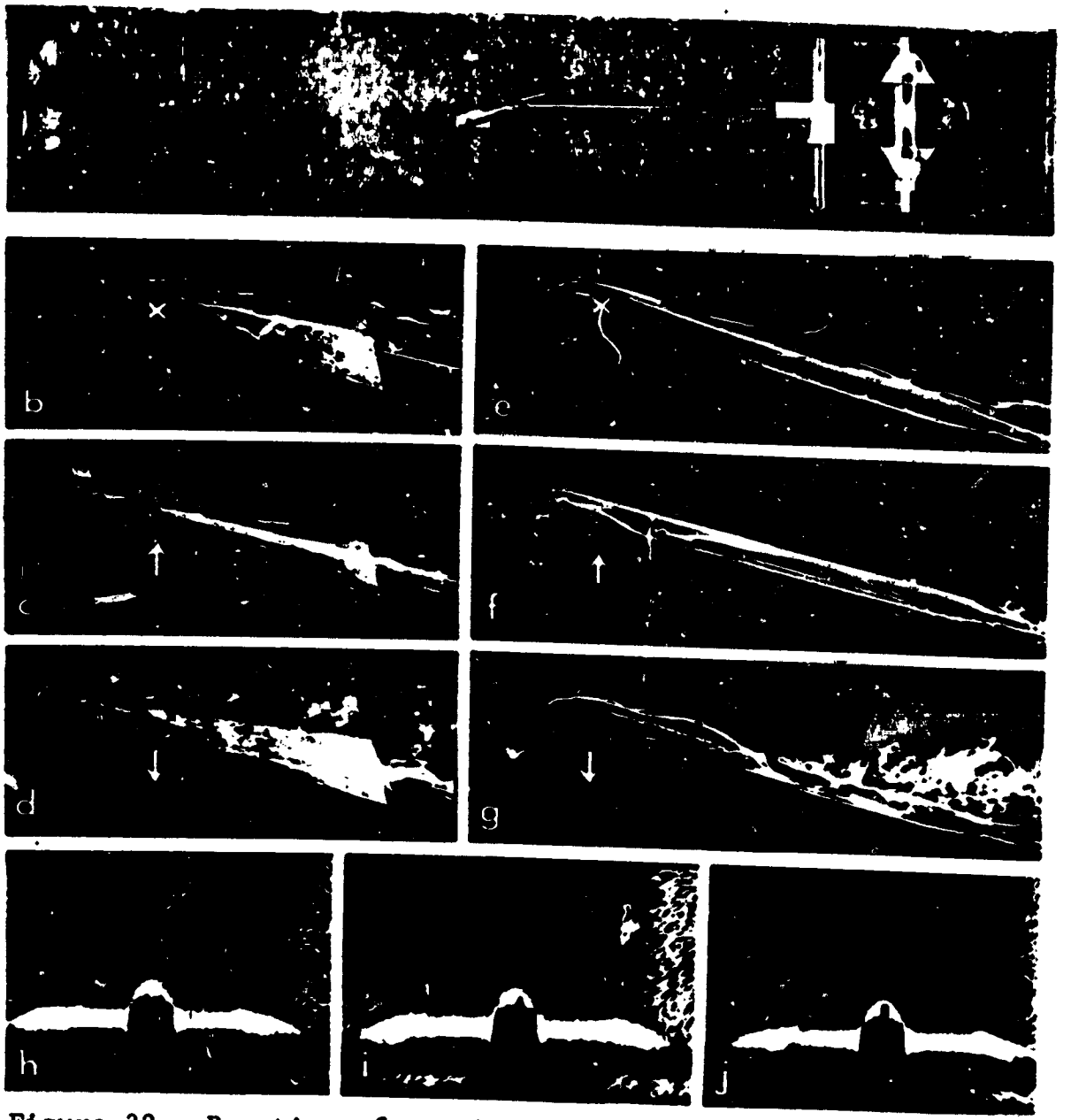

Figure 32. Bursting of vortices on thin Delta wings propelled by vertical movement (bombardment).

a) view of the test mounting adapted
b) fixed model $V_z=0$
c) ascending model $V_z=0.05\ V_o$
d) descending model $V_z=-0.2\ V_o$
e) and h) fixed model $V_z=0$
f) and i) ascending model $V_z=0.2\ V_o$
g) and j) descending model $V_z=-0.2\ V_o$

} Delta wing with sharp edges $\varphi_{BA}=60^o$; $j=0$; $i=12^o$; $l_a=100$ $Re_{l_a} \simeq 10^4$

} "Concorde" type airplane (1/280 model without jet engines); $i=12^o$ $j=0^o$; $l_a=112$; $Re_{l_a} \simeq 1.1 \cdot 10^4$

views of the outline (b, c, d, e, f and g); views of the flow in a transversal plane situated at 2/3 l_a (h, i and j)

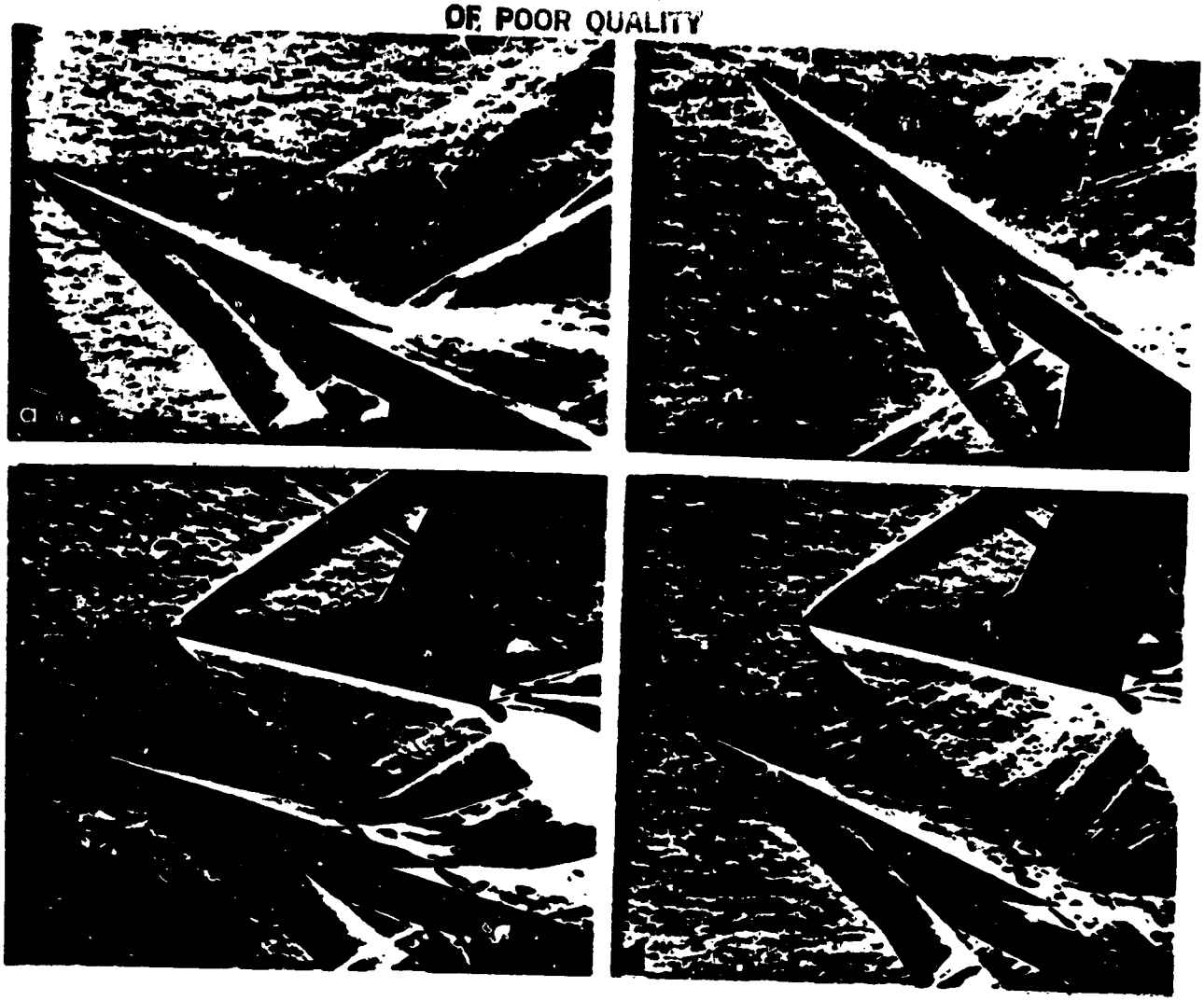

Figure 33. Flow around a thin Delta wing with supersonic incidence. Tests at Mach M_o=1.95 carried out at ONERA R1 Ch wind tunnel.

Delta wing of plate type with bevelled upper surface side edges l_a=90; φ_{BA}=75°; $Re_{l_a} \simeq 3 \cdot 10^6$; j=0°

a) i=25° } tests without dihedral
b) i=33° }
c) i=17° } tests with dihedral placed above the model ($i_{dihedral}$=12°)
d) i=25° }

} visualization by simple transversal strioscopy (position of the blades parallel to the velocity V_o)

/50

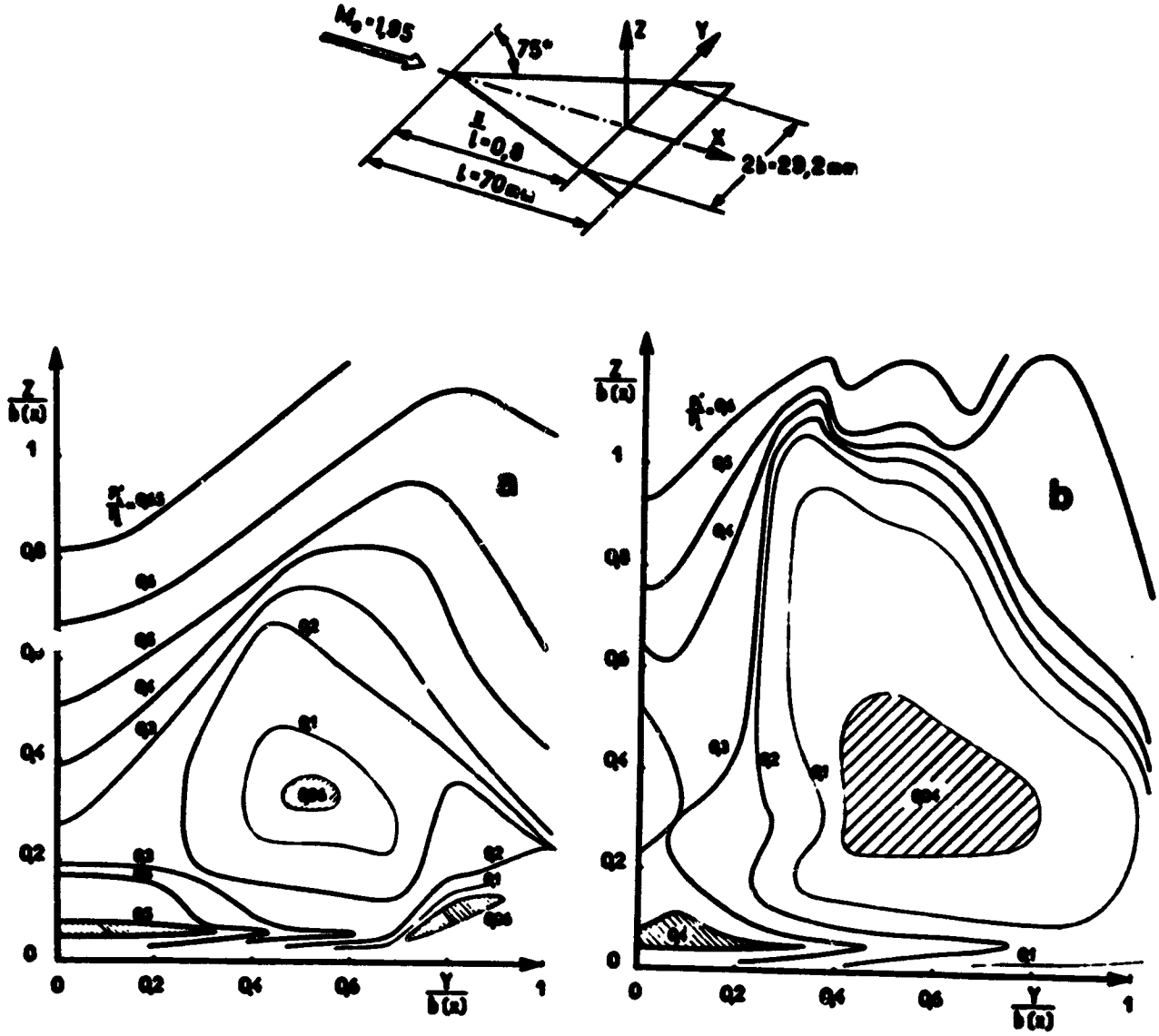

Figure 34. Supersonic bursting with the upper surface of a thin Delta wing with incidence.

Tests at Mach M_0=1.95 carried out at ONERA R1Ch wind tunnel.

Plate type Delta wing with bevelled upper surface side edges l_a=90; φ_{BA}=75°; $Re_{l_a} \simeq 3 \cdot 10^6$; j=0

a) i=25° } tests without dihedral
b) i=30° }

distribution in a transversal plane situated at approximately 80% of l_a of the stopping pressures